A CONSERVATION LAW WITH MULTIPLY DISCONTINUOUS FLUX MODELLING A FLOTATION COLUMN

RAIMUND BÜRGER

CI^{2}MA and Departamento de Ingeniería Matemática
Universidad de Concepción, Casilla 160-C, Concepción, Chile

STEFAN DIEHL

Centre for Mathematical Sciences, Lund University
P.O. Box 118, S-221 00 Lund, Sweden

MARÍA CARMEN MARTÍ *

Departamento de Matemática y Física Aplicadas
Universidad Católica de la Santísima Concepción
Casilla 297, Concepción, Chile

(Communicated by Kenneth Karlsen)

ABSTRACT. Flotation is a unit operation extensively used in the recovery of valuable minerals in mineral processing and related applications. Essential insight to the hydrodynamics of a flotation column can be obtained by studying just two phases: gas and fluid. To this end, the approach based on the drift-flux theory, proposed in similar form by several authors, is reformulated as a one-dimensional non-linear conservation law with a multiply discontinuous flux. The unknown is the gas volume fraction as a function of height and time, and the flux function depends discontinuously on spatial position due to several feed inlets. The resulting model is similar, but not equivalent, to previously studied clarifier-thickener models for solid-liquid separation and therefore adds a new real-world application to the field of conservation laws with discontinuous flux. Steady-state solutions are studied in detail, including their construction by applying an appropriate entropy condition across each flux discontinuity. This analysis leads to operating charts and tables collecting all possible steady states along with some necessary conditions for their feasibility in each case. Numerical experiments show that the transient model recovers the steady states, depending on the feed rates of the different inlets.

1. **Introduction.**

1.1. **Scope.** Flotation is a unit operation that is extensively used in the recovery of valuable minerals and coals in mineral processing but also in many other applications in environmental and chemical engineering [12, 21, 33, 36, 42]. It is a physico-chemical separation process that utilizes the difference in surface properties of the valuable hydrophobic minerals and the unwanted hydrophilic gangue material. The theory of froth flotation is complex and involves three phases (solids, water, and froth or gas) with many subprocesses [42]. The principle of the conventional flotation process is roughly as follows. Gas is introduced close to the bottom
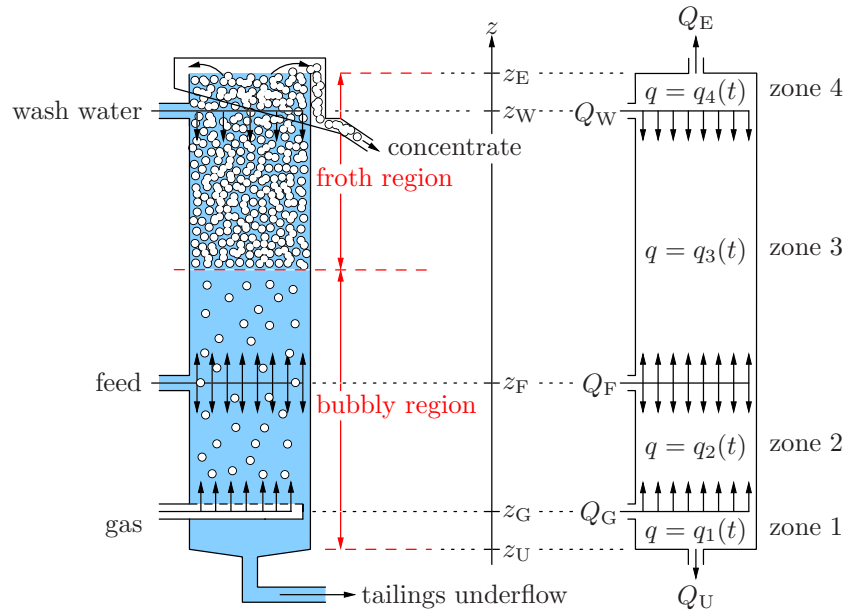
FIGURE 1. Left: Schematic of a typical flotation column (after [21, 38]), including heights of singular sources z_G, z_F and z_W, the underflow level z_U, and the effluent level z_E. Right: Corresponding conceptual model of the flotation column used in this work, indicating the volumetric feed flows Q_G, Q_F and Q_W, the underflow rate Q_U, the effluent rate Q_E, and the spatially piecewise constant bulk velocity $q = q(z, t)$.

of a flotation column (see Figure 1), and the bubbles generated then rise upward throughout the pulp that contains hydrophobic and hydrophilic solid particles. The hydrophobic particles in the pulp attach to the bubbles. Since the overall density of the bubble-particle aggregates is less than that of the medium, the aggregates then float to the top of the column, where the desired product, the foam or froth carrying the valuable material (the concentrate in mining) is removed, usually through a launder. Additionally, close to the top wash water is injected to assist with the rejection of entrained impurities [39] and to increase the froth stability and improve recovery [21, 31]. Once the hydrophobic particles have attached to the air bubbles, flotation can be considered as a separation between relatively large low-density entities, called air bubbles, and a suspension of liquid and gangue. Consequently, flotation can be described as a gas-liquid separation process by buoyancy analogous to the solid-liquid separation by gravity sedimentation in clarifier-thickeners [8, 10, 15].

Well-established spatially one-dimensional models of clarifier-thickeners can be formulated as a scalar conservation law for the local solids concentration as a function of depth and time, where the flux is discontinuous as a function of spatial position due to upward- and downward-directed bulk flows, transitions to overflow and underflow transport, and a singular source term marking the feed [8, 10, 15]. Clarifier-thickener models have motivated in part the mathematical research on conservation laws with discontinuous flux [3, 4, 6, 10, 14–20].

It is the purpose of this paper to formulate, partially analyze, solve for steady states, and numerically simulate a related model for a flotation column, where we follow [13] and limit ourselves to a one-dimensional two-phase system of gas bubbles dispersed in a fluid, or rather a suspension of liquid and gangue. Hence, we do not model any sedimentation of solid particles in the suspension. The final form of the model (cf. Figure 1) is the conservation law with multiply discontinuous flux

$$\frac{\partial \phi}{\partial t} + \frac{\partial}{\partial z} F(z, t, \phi) = \sum_{S \in \{G, F, W\}} q_S(t) \phi_S(t) \delta(z - z_S), \quad z \in \mathbb{R}, \quad t > 0, \qquad (1.1)$$

where ϕ is the sought volume fraction of gas bubbles as a function of height z and time t, and $F(z, t, \phi)$ is a flux function, made precise in later parts of the paper, that is nonlinear in ϕ and discontinuous in z at five different positions. Three of these positions, z_G, z_F and z_W, are associated with singular feed sources of gas, feed slurry, and wash water, respectively, at given rates q_S and volume fractions ϕ_S, where $\delta(\cdot)$ denotes the Dirac symbol. The model (1.1) is posed for $z \in \mathbb{R}$ without boundary conditions, and is therefore supplied solely with initial data

$$\phi(z, 0) = \phi_0(z), \quad z \in \mathbb{R}. \qquad (1.2)$$

While the time-dependent partial differential equation (PDE) (1.1) describes transient variations of ϕ as a function of position and time, a property of practical interest in applications are the stationary solutions to the model that correspond to undisturbed normal states of operation. A steady-state solution of (1.1) is generally a piecewise constant function, with possible jump discontinuities both within the four zones of Figure 1, and across the five spatial discontinuities $z = z_E$, etc.

The main outcomes of this work are to a classification of all steady-state solutions by means of diagrams and tables, and numerical simulations of dynamic behaviour. The variety of real-world applications of conservation laws with discontinuous flux is hereby widened to include flotation.

1.2. **Related work.** Our model formulation is based on the description of a flotation column by Stevenson et al. [38], Dickinson and Galvin [13], and Galvin and Dickinson [22] that is based on algebraic expressions for the gas and liquid fluxes, velocities and volume fractions. The description of one-dimensional two-phase flows based on the continuity equations for both phases and closed by defining a relative flux, or drift flux, between both phases as a function of volume fraction was introduced by Wallis [40], as is elaborated in [35]. Treatments that invoke this drift-flux analysis to describe flotation processes include [25, 27, 31, 39, 43, 44]. However, all these works utilize these variables for steady-state analyses, but do not incorporate the drift-flux variables into one solvable PDE model for transient simulations, which is precisely the main contribution of the present paper.

As stated above, the theory of conservation laws with discontinuous flux has seen a vast amount of interest in recent years, where the typical model equation is

$$\frac{\partial \phi}{\partial t} + \frac{\partial}{\partial z} \mathcal{F}(z, \phi) = 0, \quad \mathcal{F}(z, \phi) = \begin{cases} f(\phi) & \text{for } z > 0, \\ g(\phi) & \text{for } z < 0 \end{cases}$$

or equivalently, in terms of the Heaviside step function $H(z)$,

$$\frac{\partial \phi}{\partial t} + \frac{\partial}{\partial z} \big(H(z) f(\phi) + (1 - H(z)) g(\phi) \big) = 0. \qquad (1.3)$$

The basic difficulty associated with (1.3) is as follows. Suppose, for simplicity, that $\phi = \phi(z,t)$, $z \in \mathbb{R}$, $t > 0$ is a piecewise constant solution of (1.3) having traces $\phi_-(t) := \lim_{z\uparrow 0} \phi(z,t)$ and $\phi_+(t) := \lim_{z\downarrow 0} \phi(z,t)$ at $z = 0$. Then the fluxes to both sides of $z = 0$ must be equal at any time, which compels the jump condition

$$f(\phi_+(t)) = g(\phi_-(t)) \quad \text{for a.e. } t > 0. \tag{1.4}$$

This single equation does not define the two traces uniquely and one needs to specify a selection principle or jump entropy condition to single out pairs that besides satisfying (1.4) are admissible. This selection principle usually depends on the particular physical reality (1.3) is supposed to model. For instance, applications of (1.3) also include traffic flow with discontinuously changing road surface conditions, ion etching, two-phase flow in heterogeneous porous media, and medical applications (see [5], [24, Ch. 8], and [28] for overviews and references). We use here the admissibility condition from [14], which has proved to be the natural one for the related problem of continuous sedimentation [15]. Furthermore, its generalization [18] to the case of a scalar convection-diffusion equation with spatial discontinuity in both the flux and diffusion functions implies the physically relevant solution in the case of the well-established model of continuous sedimentation with compression [10]. As is stated in [24, p. 426], there are different "recipes" to select unique solutions of the Riemann problem of (1.3), and all of them eventually lead to uniqueness of the initial value problem for (1.3), according to the unified treatment in [1].

1.3. **Outline of the paper.** In Section 2, we derive the model equations for the local fraction of gas bubbles, detailing the definition of the flux density functions in each zone of the spatial domain and the treatment of the feed inlets. Some notation necessary for the description of the steady-state solutions is also introduced. In Section 3, we focus on the characterization of all possible steady states for the flotation model previously defined, providing a detailed study of the derivation process at the different spatial discontinuities introduced by the feed inlets. Some steady states exist only under certain conditions on the injection rates and to get an overview of all possibilities, we present operating charts and tables for the categorization of all steady states. In Section 4, we briefly review the numerical method to approximately solve the flotation model. Some numerical examples are provided in Section 5 and, finally, we present some conclusions in Section 6.

2. **Mathematical model.**

2.1. **Phase velocities and drift flux.** Assume that we consider a region of space that is free of sources and sinks, that ϕ is the local fraction of gas bubbles, and that $\boldsymbol{v}_\mathrm{f}$ and $\boldsymbol{v}_\mathrm{g}$ are the phase velocities of the gas and fluid, respectively. Then the conservation of mass equations for both can be written in local form as

$$\frac{\partial \phi}{\partial t} + \nabla \cdot (\phi \boldsymbol{v}_\mathrm{g}) = 0, \qquad \frac{\partial (1-\phi)}{\partial t} + \nabla \cdot \big((1-\phi)\boldsymbol{v}_\mathrm{f}\big) = 0, \tag{2.1}$$

where we assume that the gas bubbles are incompressible and do not coalesce. Then, defining the volume average velocity, or bulk flux of the suspension,

$$\boldsymbol{q} := \phi \boldsymbol{v}_\mathrm{g} + (1-\phi)\boldsymbol{v}_\mathrm{f} \tag{2.2}$$

and the gas-fluid relative velocity $\boldsymbol{v}_\mathrm{r} := \boldsymbol{v}_\mathrm{g} - \boldsymbol{v}_\mathrm{f}$, we may rewrite the first equation in (2.1) and replace the second by the sum of both to obtain

$$\frac{\partial \phi}{\partial t} + \nabla \cdot \big(\phi \boldsymbol{q} + \phi(1-\phi)\boldsymbol{v}_\mathrm{r}\big) = 0, \qquad \nabla \cdot \boldsymbol{q} = 0.$$

It is assumed that $\boldsymbol{v}_r = v_r \boldsymbol{e}_z$, where $\boldsymbol{e}_z$ is the upward-pointing unit vector and v_r is given as a function of ϕ so that the gas drift-flux function is

$$j_g(\phi) := \phi(1 - \phi)v_r(\phi) = \phi v_{\text{term}} V(\phi). \tag{2.3}$$

The drift-flux function $j_g(\phi)$ gives the gas flux in a closed column relative to the column. Here, v_{term} is the terminal velocity of a single bubble in an unbounded fluid. As is stated in [38], there exists a number of methods to calculate v_{term}, and Wallis' generalized correlation [41] leading to v_{term} is recommended, see [38, Appendix A] for details. This correlation involves additional quantities such as equilibrium surface tension and the viscosity of the fluid. Its detailed discussion is beyond the focus of this paper; for the present analysis it suffices to assume that v_{term} is a set constant for a given material and equipment.

Furthermore, in (2.3), $V(\phi)$ is a dimensionless hindered-bubbling function that can, for instance, be given by the Richardson-Zaki expression [34]

$$V(\phi) = (1 - \phi)^{n_{\text{RZ}}}, \quad n_{\text{RZ}} \geq 0. \tag{2.4}$$

The maximum possible volume fraction of bubbles is $\phi_{\max} = 1$. Realistic values of n_{RZ} range from $n_{\text{RZ}} = 2$ to $n_{\text{RZ}} = 3.2$ (cf., e.g., [13, 22, 25, 31, 39]).

Finally, in one space dimension (in the z-direction) and away from sinks or sources, $\nabla \cdot \boldsymbol{q} = 0$ reduces to $\partial q/\partial z = 0$, so q will depend on t only, and the only equation that needs to be solved is the nonlinear first-order conservation law

$$\frac{\partial \phi}{\partial t} + \frac{\partial}{\partial z} j(\phi, t) = 0, \quad \text{where } j(\phi, t) := q(t)\phi + j_g(\phi). \tag{2.5}$$

Hence, $j(\phi, t)$ is the total flux of gas. If we denote the total fluid flux by $\varphi := (1 - \phi)v_f$, then (2.2) yields the simple relation $q = j + \varphi$ between the three fluxes, which all generally may have any sign.

2.2. **Volumetric flows, bulk velocities and flux functions.** It is assumed that the unit has a constant cross-sectional area A, and that concentrations are horizontally constant so that all variables depend on height z and time t only. The unit is fed at heights $z = z_W$, $z = z_F$ and $z = z_G$, with wash water, fluid (feed slurry), and gas, respectively (see Figure 1), where we assume that $z_W > z_F > z_G$. The corresponding volumetric flows $Q_W \geq 0$, $Q_F \geq 0$ and $Q_G \geq 0$ are assumed to be given functions of time, as is the volumetric underflow rate $Q_U \geq 0$. Furthermore, Q_E is the resulting effluent volumetric overflow, which is assumed to be nonnegative, i.e., the mixture is conserved and the vessel is always completely filled with mixture.

The spatially piecewise constant bulk velocity $q = q(z, t)$ is defined by the values $q_1(t)$ to $q_4(t)$ in the corresponding four zones in the vessel; see Figure 1. To simplify notation, we define the velocities $q_S(t) := Q_S(t)/A$ for $S \in \{E, F, G, U, W\}$.

Starting from the bottom of the vessel, we have $q_1 = -q_U$, $q_2 = q_1 + q_G$, etc. and we obtain the total bulk velocity function

$$q(z, t) := \begin{cases} q_1 = -q_U & \text{for } z < z_G, \\ q_2 = q_G - q_U & \text{for } z_G \leq z < z_F, \\ q_3 = q_G + q_F - q_U & \text{for } z_F \leq z < z_W, \\ q_4 = q_G + q_F + q_W - q_U & \text{for } z \geq z_W. \end{cases} \tag{2.6}$$

Hence, we always have $q_E = q_4 \geq 0$ and $q_1 = -q_U \leq 0$, whereas q_2 and q_3 may have any sign.

We denote the intervals $z > z_E$ and $z < z_U$ by the effluent and underflow zone, respectively. During normal operation, zone 1 contains only liquid. Above $z = z_G$ there is a region of bubbles rising with a high velocity up to an upper region of froth with a high volume fraction of gas; see Figure 1. The large discontinuity between the bubbly and froth regions is usually located in the interval $[z_F, z_W]$, either at the location of one injection point or within a zone. As we will see, discontinuities in ϕ are possible at every injection point and inside some zones. Usually, zone 4 is small, and sometimes $z_G = z_F$, i.e., gas and feed slurry are injected at the same location.

We assume that in the effluent and underflow zones, the gas and the fluid move at the same velocity, so we set $v_r := 0$, and therefore $j_g := 0$ in these zones. The total flux function is then defined as

$$F(z,t,\phi) := \begin{cases} j_U(\phi,t) := q_1(t)\phi & \text{for } z < z_U, \\ j_1(\phi,t) := q_1(t)\phi + j_g(\phi) & \text{for } z_U \le z < z_G, \\ j_2(\phi,t) := q_2(t)\phi + j_g(\phi) & \text{for } z_G \le z < z_F, \\ j_3(\phi,t) := q_3(t)\phi + j_g(\phi) & \text{for } z_F \le z < z_W, \\ j_4(\phi,t) := q_4(t)\phi + j_g(\phi) & \text{for } z_W \le z < z_E, \\ j_E(\phi,t) := q_4(t)\phi & \text{for } z \ge z_E. \end{cases} \tag{2.7}$$

2.3. **Feed sources and governing equation in final form.** The conservation law (2.5) is completed by including the feed of material at levels z_W, z_F and z_G at volume rates Q_W, Q_F and Q_G. The feed mechanisms give rise to singular source terms that extend (2.5) to the final governing model equation (1.1). The given gas volume fraction of the three time-dependent feed streams is denoted by ϕ_W, ϕ_F and ϕ_G, respectively. In agreement to common practice, we assume that either pure gas or pure liquid is injected through the respective singular sources, so we assume from now on $\phi_G \equiv 1$ and $\phi_F = \phi_W \equiv 0$.

2.4. **Entropy solutions.** Within each zone, the governing equation (1.1), (2.7) reduces to (2.5), and we consider the Cauchy problem of this equation. A piecewise smooth function $\phi = \phi(x,t)$ is defined to be an *entropy solution* of the problem if ϕ is continuously differentiable everywhere with the exception of a finite number of curves $z = z_d(t) \in C^1$ of discontinuities. At each point $(z_d(t), t)$ of discontinuity, the (non-equal) values $\phi^\pm := \phi(z_d(t)^\pm, t)$ satisfy the jump condition

$$z_d'(t) = S(\phi^+, \phi^-) := \frac{f(\phi^+) - f(\phi^-)}{\phi^+ - \phi^-}, \tag{2.8}$$

and the jump entropy condition

$$S(u, \phi_-) \ge S(\phi_+, \phi_-) \quad \text{for all } u \text{ between } \phi^+ \text{ and } \phi^-. \tag{2.9}$$

It is well known that entropy solutions in the sense of Oleinik [30] are also the unique entropy solutions in the sense of Kružkov-type [26] integral inequalities (cf., e.g., [24]). On the other hand and as mentioned in Section 1.2, at the five spatial discontinuities of problem (1.1), a generalized entropy is needed [14, 18]. Since we only construct steady-state solutions, we review that condition in Section 3.1 for this purpose, which means less notation than for the dynamic case.

2.5. **Properties of the zone flux functions.** We assume that the drift-flux function $j_g(\phi) \ge 0$ is continuously differentiable, satisfies $j_g(0) = j_g(1) = 0$, and is concave-convex with an inflection point $\phi_{infl} \in (0,1)$; see Figure 2. (Drawings have been made for j_g given by (2.3) and (2.4), with $v_{term} = 2.7\,\text{cm/s}$ and $n_{RZ} = 3.2$.
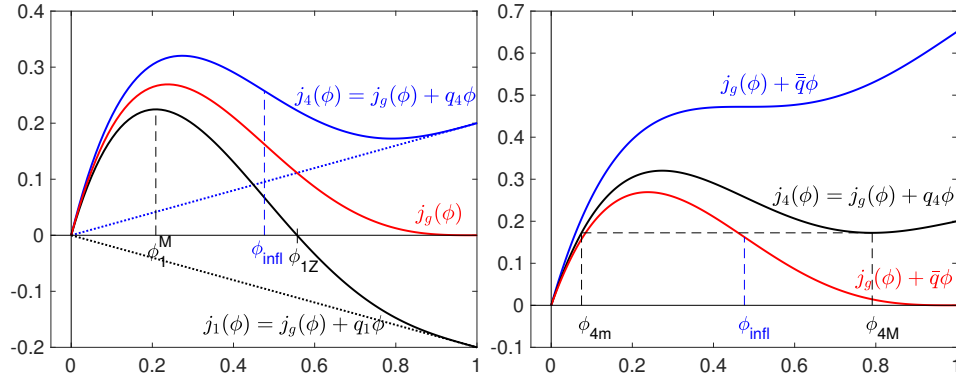
FIGURE 2. Flux functions' properties and specific volume fraction. Left: Drift-flux function j_g and flux curves for zones 1 and 4. Right: The local minimum ϕ_M and appurtenant ϕ_m for a zone flux j with positive q, and flux curves with zero derivatives at $\phi_{\max} = 1$ and ϕ_infl. In these and other plots, we have used the expression (2.4) with $n_\mathrm{RZ} = 3.2$ in the drift-flux function j_g. The unit on the vertical axis is cm/s.

These values are also utilized in [13].) The form of j_g singles out certain distinguished values of the volume fraction that appear in the steady-state solution (see Figure 2). The same values appear in the related problem of continuous sedimentation [16, 17].

Since we will mostly refer to steady-state situations, we often supress the dependence on t in $j_1, \ldots, j_4$. The functions $j_1, \ldots, j_4$ and j_g have the same inflection point ϕ_infl, since they only differ by a linear term. If $j_k(\phi)$ has a zero in $(0, 1]$, which can happen only for $k = 1, 2, 3$ and $q_k < 0$, then we denote it by $\phi_{k\mathrm{Z}}$. If $j_k(\phi) < 0$ for all $\phi \in (0, 1]$, we set $\phi_{k\mathrm{Z}} := 0$. We define

$$\bar{q} := -j_\mathrm{g}'(1), \qquad \bar{\bar{q}} := -j_\mathrm{g}'(\phi_\mathrm{infl}),$$

which are the bulk velocities such that the slope of $j_k(\phi)$ is zero at $\phi_{\max} = 1$ and ϕ_infl, respectively. To reduce the number of cases to investigate, we assume in this work that

$$\bar{q} = -j_\mathrm{g}'(1) = 0, \tag{2.10}$$

in accordance with the common Richardson-Zaki function (2.4). For intermediate values of q_k, i.e., $\bar{q} < q_k < \bar{\bar{q}}$, there is a local minimizer $\phi_{k\mathrm{M}}$ of $j_k(\phi)$ $(k = 2, 3, 4)$ on the right of ϕ_infl. Then $0 = j_k'(\phi_{k\mathrm{M}}) = j_\mathrm{g}'(\phi_{k\mathrm{M}}) + q_k$. To obtain a definition for all values of q_k, we note that the restriction $(j_\mathrm{g}|_{(\phi_\mathrm{infl}, 1)})'$ is a decreasing function so that we can define

$$\phi_{k\mathrm{M}} := \begin{cases} 1 & \text{if } q_k \leq \bar{q}, \\ ((j_\mathrm{g}|_{(\phi_\mathrm{infl}, 1)})')^{-1}(-q_k) & \text{if } \bar{q} < q_k < \bar{\bar{q}}, \\ \phi_\mathrm{infl} & \text{if } q_k \geq \bar{\bar{q}}. \end{cases}$$

Given $\phi_{k\mathrm{M}}$ and $q_k \geq 0$, we define $\phi_{k\mathrm{m}}$ as the unique value satisfying

$$j_k(\phi_{k\mathrm{m}}) = j_k(\phi_{k\mathrm{M}}), \quad 0 \leq \phi_{k\mathrm{m}} \leq \phi_\mathrm{infl}.$$

For $q_k < \bar{\bar{q}}$, $j_k(\phi)$ assumes a local maximum point at $\phi_k^{\mathrm{M}} \in [0, \phi_{\mathrm{infl}})$. Let $q_{\mathrm{neg}} := -j_{\mathrm{g}}'(0)$ be the value below which j_k is a decreasing function. For $q_k \leq q_{\mathrm{neg}}$, the local maximum is $\phi_k^{\mathrm{M}} := 0$. For $q_k \geq \bar{\bar{q}}$, we set $\phi_k^{\mathrm{M}} := \phi_{\mathrm{infl}}$.

In some instances it is convenient to write out the dependence on q of the flux function, i.e., $j_k(\phi; q_k)$, and of the specific concentrations, e.g., $\phi_k^{\mathrm{M}}(q_k)$. The following properties follow directly from the definitions above (cf. [16, Lemma 2]).

Lemma 2.1. *The following properties hold:*

$$\frac{\mathrm{d}}{\mathrm{d}q_k} j_k(\phi_{k\mathrm{M}}(q_k); q_k) = \phi_{k\mathrm{M}}(q_k), \qquad \frac{\mathrm{d}}{\mathrm{d}q_k} j_k(\phi_k^{\mathrm{M}}(q_k); q_k) = \phi_k^{\mathrm{M}}(q_k).$$

3. **Steady-state solutions.** In order to completely describe all possible steady states of model (1.1) (under the assumptions of Section 2.5), we here extract from the theory of conservation laws with discontinuous flux function [14, 18] what is necessary to construct steady-state solutions in a neighbourhood of a spatial discontinuity.

To start with, we investigate the case when the steady-state solution is constant ϕ_k in zone $k = 1, 2, 3, 4$, and constant ϕ_{U} and ϕ_{E} in the underflow and effluent zones, respectively. In Section 3.9, we describe the general solution, having also discontinuities within one or several zones. First, we review the necessary theory and notation, and then go through the possible couplings between zones 1 to 4 and the effluent and underflow zones.

3.1. **Construction of steady-state solutions for a conservation law with discontinuous flux function.** We consider the conservation law with discontinuous flux function (1.3). The equation should be interpreted in the weak sense and we seek steady-state solutions of the form

$$\phi(z) = \begin{cases} \phi_- & \text{if } z < 0, \\ \phi_+ & \text{if } z > 0, \end{cases}$$

where $\phi_{\pm}$ are constants. The conservation law across $z = 0$ implies the jump condition $g(\phi_-) = f(\phi_+)$ (see (1.4)). This single equation has two unknowns. The generalized entropy condition [14] selects the physically relevant solution in a neighbourhood of $z = 0$ for a dynamic solution of (1.3) for given initial data at $t = 0$. We define the auxiliary functions

$$\hat{f}(\phi; \phi_+) := \begin{cases} \displaystyle\min_{v \in [\phi, \phi_+]} f(v) & \text{if } \phi \leq \phi_+, \\ \displaystyle\max_{v \in [\phi_+, \phi]} f(v) & \text{if } \phi > \phi_+, \end{cases}$$

$$\check{g}(\phi; \phi_-) := \left. \begin{cases} \displaystyle\max_{v \in [\phi, \phi_-]} g(v) & \text{if } \phi \leq \phi_-, \\ \displaystyle\min_{v \in [\phi_-, \phi]} g(v) & \text{if } \phi > \phi_- \end{cases} \right\} = \hat{g}(\phi_-; \phi).$$

Since $\check{g}(\cdot; \phi_-)$ is non-increasing and $\hat{f}(\cdot; \phi_+)$ is non-decreasing, the intersection of the graphs of these functions occurs at a unique flux value, if there exists an intersection. For the model of flotation, this is always the case; the proof of this statement can be made in the same way as for the problem of continuous sedimentation; see [15].

We define the set of possible ϕ-values of the intersection as

$$\bar{\Phi} = \bar{\Phi}(\phi_+, \phi_-) := \left\{ \phi \in [0, 1] : \hat{f}(\phi; \phi_+) = \check{g}(\phi; \phi_-) \right\}$$

and the corresponding unique flux value $\eta(\phi_+, \phi_-) := \hat{f}(\bar{\Phi}; \phi_+)$. Since we are here only interested in stationary solutions, the generalized entropy condition can be stated as

$$\hat{f}(\phi_+; \phi_+) = \eta(\phi_+, \phi_-) = \check{g}(\phi_-; \phi_-), \tag{3.1}$$

where we note that $\hat{f}(\phi_+; \phi_+) = f(\phi_+)$ and $\check{g}(\phi_-; \phi_-) = g(\phi_-)$.

3.2. **Couplings at the underflow location** $z = z_{\mathrm{U}}$. In a neighbourhood of $z = z_{\mathrm{U}}$, the PDE (1.1) becomes

$$\frac{\partial \phi}{\partial t} + \frac{\partial}{\partial z} F(z, t, \phi) = 0,$$

where

$$F(z, t, \phi) = \begin{cases} j_{\mathrm{U}}(\phi, t) = q_1(t)\phi & \text{if } z < z_{\mathrm{U}}, \\ j_1(\phi, t) = q_1(t)\phi + j_{\mathrm{g}}(\phi) & \text{if } z > z_{\mathrm{U}}. \end{cases}$$

We now suppress the time dependence and seek possible constant solutions ϕ_1 and ϕ_{U} in the two neighbouring zones so that the entropy condition (3.1) is satisfied. With the notation of Section 3.1, we have $g(\phi) = j_{\mathrm{U}}(\phi) = q_1\phi$ and $f(\phi) = j_1(\phi) = q_1\phi + j_{\mathrm{g}}(\phi)$. The task is to find a pair ϕ_{U} and ϕ_1 so that the entropy condition (3.1) is satisfied. This condition now reads

$$\hat{j}_1(\phi_1; \phi_1) = \eta(\phi_1, \phi_{\mathrm{U}}) = \check{j}_{\mathrm{U}}(\phi_{\mathrm{U}}; \phi_{\mathrm{U}}), \tag{3.2}$$

where $\eta(\phi_1, \phi_{\mathrm{U}})$ denotes the flux value of the intersection of $\check{j}_{\mathrm{U}}(\cdot; \phi_{\mathrm{U}})$ and $\hat{j}_1(\cdot; \phi_1)$. As $j_{\mathrm{U}}(\phi) = -q_{\mathrm{U}}\phi$ is a linear decreasing function, we have $\check{j}_{\mathrm{U}}(\cdot; \phi_{\mathrm{U}}) = j_{\mathrm{U}}$ for any $\phi_{\mathrm{U}} \in [0, 1]$. The function j_1 has two monotonicity intervals separated by the maximum point ϕ_1^{M}, which leads to the following cases:

(a) $\phi_1 \in [0, \phi_1^{\mathrm{M}}]$, see Fig. 3(a). The only possible intersection between $\hat{j}_1$ and $\check{j}_{\mathrm{U}}$ is $\phi_1 = 0$; hence $\phi_{\mathrm{U}} = 0$. Thus, the zero solution on both sides is the only possible steady-state coupling in this case.

(b) $\phi_1 \in (\phi_1^{\mathrm{M}}, 1]$, see Fig. 3(b1) and (b2). If $\phi_1 \in (\phi_1^{\mathrm{M}}, \phi_{1\mathrm{Z}})$, the middle plot shows that the only possible intersection is, as in the previous case, $\phi_1 = 0$, but is outside the interval of definition of ϕ_1, i.e., there is no possible steady state with $\phi_1 \in (\phi_1^{\mathrm{M}}, \phi_{1\mathrm{Z}})$. If $\phi_1 \in [\phi_{1\mathrm{Z}}, 1]$ (right plot), then there is always a possible intersection between $\hat{j}_1(\cdot; \phi_1)$ and $\check{j}_{\mathrm{U}}(\cdot; \phi_{\mathrm{U}})$ satisfying (3.2). Consequently, the possible steady states satisfy $\phi_1 \in [\phi_{1\mathrm{Z}}, 1]$ and $\phi_{\mathrm{U}} \in [0, 1]$.

We conclude this subsection by stating the possible steady-state values in the underflow and the first zone:

$$\phi_{\mathrm{U}} \in [0, 1], \quad \phi_1 \in \{0\} \cup [\phi_{1\mathrm{Z}}, 1]. \tag{3.3}$$

3.3. **Couplings at the effluent location** $z = z_{\mathrm{E}}$. Here, $j_{\mathrm{E}}(\phi) = q_{\mathrm{E}}\phi$ is an increasing linear function. The procedure is analogous to the coupling at $z = z_{\mathrm{U}}$. In fact, this case is the same as the one at the underflow level in the problem of continuous sedimentation. Details can be found in [15, Section 9], and we state here directly the possible steady-state values in zone 4 and the effluent zone:

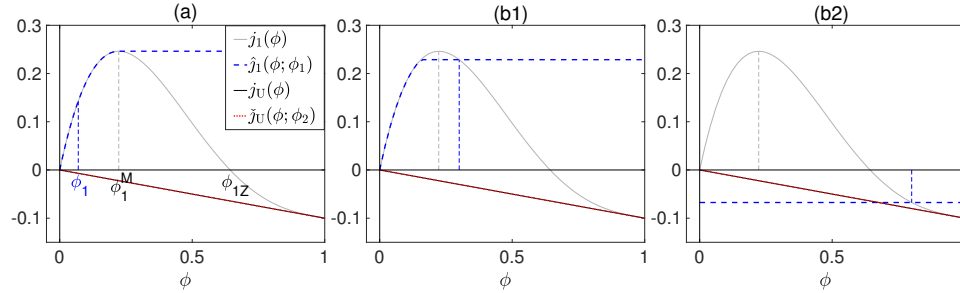$$\phi_4 \in [0, \phi_{4\mathrm{m}}] \cup [\phi_{4\mathrm{M}}, 1], \quad \phi_{\mathrm{E}} \in [0, 1]. \tag{3.4}$$

FIGURE 3. The decreasing function $\check{j}_{\mathrm{U}}(\cdot; \phi_{\mathrm{U}}) = j_{\mathrm{U}}$ and three possible cases of graphs of $\hat{j}_1(\cdot; \phi_1)$ depending on ϕ_1. The intersection of $\hat{j}_1(\cdot; \phi_1)$ and j_{U} defines the possible values in a steady-state solution.

3.4. **Couplings at** $z = z_{\mathrm{G}}$. In a neighbourhood of $z = z_{\mathrm{G}}$, the PDE (1.1) is

$$\frac{\partial \phi}{\partial t} + \frac{\partial}{\partial z}\big((1 - H(z - z_{\mathrm{G}}))j_1(\phi, t) + H(z - z_{\mathrm{G}})j_2(\phi, t)\big) = q_{\mathrm{G}}(t)\phi_{\mathrm{G}}(t)\delta(z - z_{\mathrm{G}}),$$

which, with $\phi_{\mathrm{G}}(t) \equiv 1$, is formally equivalent to

$$\frac{\partial \phi}{\partial t} + \frac{\partial}{\partial z}\big((1 - H(z - z_{\mathrm{G}}))(j_1(\phi, t) + q_{\mathrm{G}}(t)) + H(z - z_{\mathrm{G}})j_2(\phi, t)\big) = 0.$$

The flux functions to consider for the steady-state coupling are thus

$$j_1(\phi) + q_{\mathrm{G}} = j_{\mathrm{g}}(\phi) - q_{\mathrm{U}}\phi + q_{\mathrm{G}} \qquad \text{for} \quad z < z_{\mathrm{G}},$$
$$j_2(\phi) = j_{\mathrm{g}}(\phi) + (q_{\mathrm{G}} - q_{\mathrm{U}})\phi \quad \text{for} \quad z > z_{\mathrm{G}},$$

which intersect only at $\phi = 1$, and the entropy condition is

$$\hat{j}_2(\phi_2; \phi_2) = \eta(\phi_1, \phi_2) = \check{j}_1(\phi_1; \phi_1) + q_{\mathrm{G}}.$$

We have $q_1 = -q_{\mathrm{U}} \leq 0$, but q_2 may have any sign. We will make a main division depending on the sign of q_2. From (3.3), we know that a steady state in zone 1 satisfies $\phi_1 \in \{0\} \cup [\phi_{1\mathrm{Z}}, 1]$. These two intervals should be coupled with the three monotonicity intervals of j_2, which are separated by ϕ_2^{M} and $\phi_{2\mathrm{M}}$. We will get conditions on q_{G} in the subcases.

Remark 1. In the division into subcases further on, we will sometimes let such overlap in the following way. Instead of having disjoint intervals defining two subcases, e.g., $\phi_2 \in [0, \phi_2^{\mathrm{M}}]$ and $\phi_2 \in (\phi_2^{\mathrm{M}}, \phi_{2\mathrm{M}})$, the second subcase will instead be $\phi_2 \in [\phi_2^{\mathrm{M}}, \phi_{2\mathrm{M}}]$. This overlap will reduce the number of conditions in terms of inequalities. Then the same steady-state solution can occur in two subcases, but the final number of steady-state solutions is not affected.

1. **Case G1.** $q_1 \leq 0 \leq q_2$.
   (a) $\phi_1 = 0$, $\phi_2 \in [0, \phi_2^{\mathrm{M}}]$; see Fig. 4(a). A necessary condition for a steady-state solution is

   $$j_2(\phi_2^{\mathrm{M}}) \geq q_{\mathrm{G}}. \tag{G}$$

   (b) $\phi_1 = 0$, $\phi_2 \in [\phi_2^{\mathrm{M}}, \phi_{2\mathrm{M}}]$; see Fig. 4(b). A necessary condition for a steady-state solution is (G).
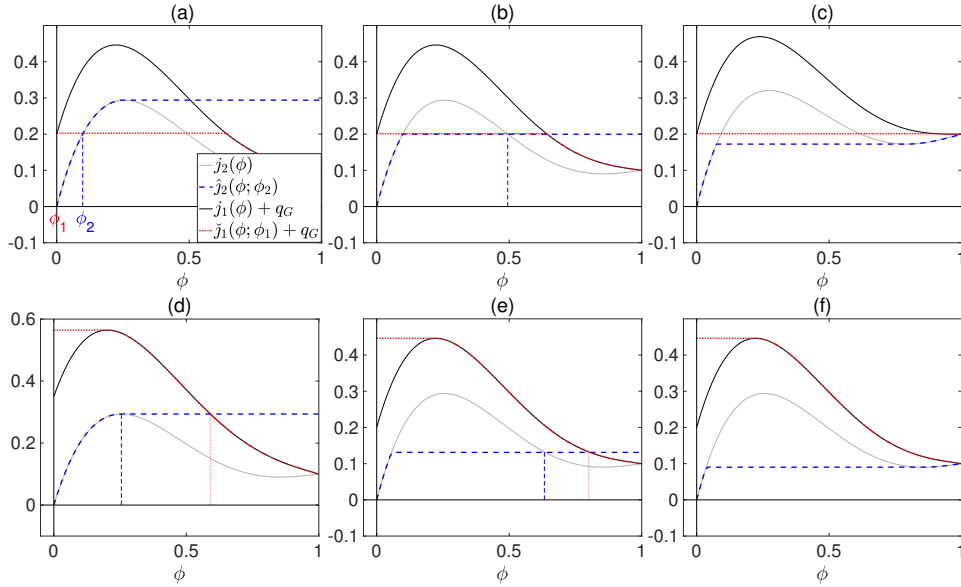
FIGURE 4. Case G1: $q_1 \leq 0 \leq q_2$. Possible steady-state values for zones 1 and 2. The gas injection velocity is set to $q_G = 0.2\,\mathrm{cm/s}$ in all subplots except for (d) where it is $0.35\,\mathrm{cm/s}$.

(c) $\phi_1 = 0$, $\phi_2 \in (\phi_{2M}, 1]$; see Fig. 4(c). The only possible solution is $\phi_2 = 1$ when $q_1 = 0$.

(d) $\phi_1 \in [\phi_{1Z}, 1]$, $\phi_2 \in [0, \phi_2^M]$; see Fig. 4(d). The only possible steady-state solution satisfies $\phi_2 = \phi_2^M < \phi_1$.

(e) $\phi_1 \in [\phi_{1Z}, 1]$, $\phi_2 \in (\phi_2^M, \phi_{2M})$; see Fig. 4(e). A steady-state coupling is possible with $\phi_2 \leq \phi_1$ with equality if and only if $q_1 = q_2$, i.e., $q_G = 0$.

(f) $\phi_1 \in [\phi_{1Z}, 1]$, $\phi_2 \in [\phi_{2M}, 1]$; see Fig. 4(f). The only possible coupling is $\phi_1 = \phi_2 = 1$.

2. **Case G2.** $q_1 \leq q_2 \leq 0$.

(a) $\phi_1 = 0$, $\phi_2 \in [0, \phi_2^M]$; see Fig. 5(a). The same as Case G1(a) with condition (G).

(b) $\phi_1 = 0$, $\phi_2 \in [\phi_2^M, 1]$; see Fig. 5(b1) and (b2). As in Case G1(b) a necessary condition is (G). The largest value in zone 2 is $\phi_2 = \phi_{2Z}$ and then $q_1 = q_2$, i.e., $q_G = 0$, see plot (b2).

(c) $\phi_1 \in [\phi_{1Z}, 1]$, $\phi_2 \in [0, \phi_2^M]$; see Fig. 5(c). The same as Case G1(d): $\phi_2 = \phi_2^M < \phi_1$.

(d) $\phi_1 \in [\phi_{1Z}, 1]$, $\phi_2 \in (\phi_2^M, 1]$. Solution exists with either a positive, see Fig. 5(d1) or a negative flux (d2).

3.5. **Couplings at $z = z_F$.** We derive the possible constant steady states in zones 2 and 3 considering their coupling at $z = z_F$. This is the most complicated case where both bulk velocities, hence both fluxes, can be either positive or negative. Since there is no injection of bubbles, $\phi_F = 0$, the fluxes to consider are

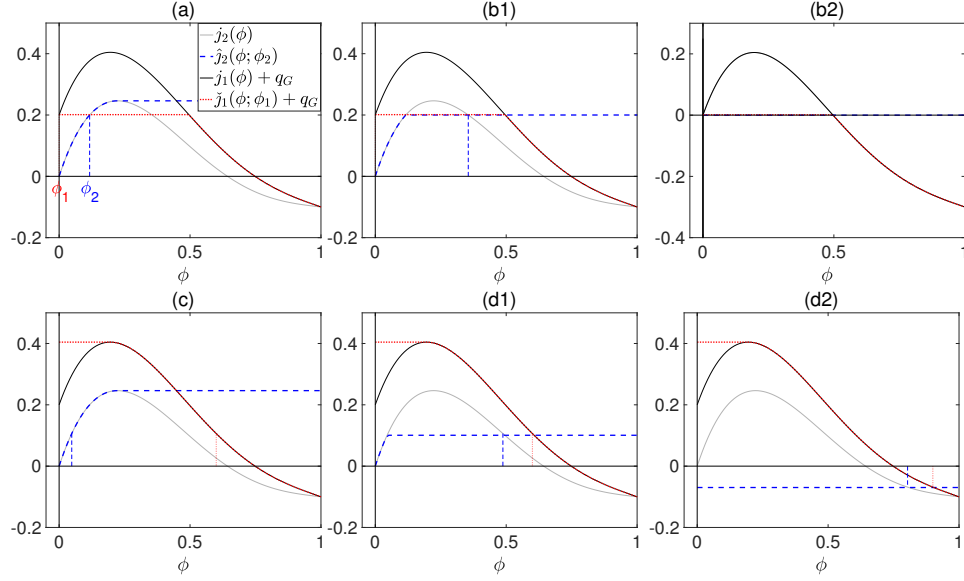$$j_2(\phi) = q_2\phi + j_g(\phi), \quad z < z_F,$$

FIGURE 5. Case G2: $q_1 \leq q_2 \leq 0$. Possible steady-state values for zones 1 and 2. The value of q_G is set to $q_G = 0.2\,\mathrm{cm/s}$ except for plot (b2), where it is $0\,\mathrm{cm/s}$.

$$j_3(\phi) = q_3\phi + j_g(\phi), \quad z > z_F,$$

where $q_2 = q_G - q_U \leq q_G + q_F - q_U = q_3$. We require that the entropy condition (3.1) holds, which now reads

$$\hat{j}_3(\phi_3; \phi_3) = \eta(\phi_3, \phi_2) = \check{j}_2(\phi_2; \phi_2). \tag{3.5}$$

We now study the possible intersections between $\check{j}_2(\cdot; \phi_2)$ and $\hat{j}_3(\cdot; \phi_3)$ and make a division into three main cases F1–F3 depending on the signs of the two bulk velocities q_2 and q_3. Subdivisions are then made according to the intervals of monotonicity of the flux functions j_2 and j_3, which give qualitatively different intersections of $\check{j}_2(\cdot; \phi_2)$ and $\hat{j}_3(\cdot; \phi_3)$ because of their strictly monotone parts and plateaus. Some cases will be empty, i.e., no steady-state solution is possible and this may depend on q_2 and q_3. When a steady-state solution is possible, it always satisfies $j_2(\phi_2) = j_3(\phi_3)$.

1. **Case F1.** $0 \leq q_2 \leq q_3$.
   (a) $\phi_2 \in [0, \phi_2^M]$, $\phi_3 \in [0, \phi_3^M]$; see Fig. 6(a). In this case there is a possible intersection point between $\check{j}_2(\cdot; \phi_2)$ and $\hat{j}_3(\cdot; \phi_3)$. We have $q_2 \leq q_3 \Leftrightarrow \phi_3 \leq \phi_2$.
   (b) $\phi_2 \in (\phi_2^M, \phi_{2M})$, $\phi_3 \in [0, \phi_3^M]$. The flux value of the intersection of $\check{j}_2$ and $\hat{j}_3$ is $\eta = j_2(\phi_2^M) = \check{j}_2(\phi_2^M; \phi_2)$. Since this case requires $\phi_2^M < \phi_2$, (3.5) is not satisfied and there is no possible stationary solution.
   (c) $\phi_2 \in [\phi_{2M}, 1]$, $\phi_3 \in [0, \phi_3^M]$; see Fig. 6(c). The only possibility for the plateau of $\check{j}_2(\cdot; \phi_2)$ to intersect the increasing part of $\hat{j}_3(\cdot; \phi_3)$ is that the plateau lies above the value of the local maximum of j_2. In other words,

this case is empty unless the following condition is satisfied:

$$j_2(1) \geq j_2(\phi_2^{\mathrm{M}}). \tag{FI}$$

(d) $\phi_2 \in [0, \phi_2^{\mathrm{M}}]$, $\phi_3 \in (\phi_3^{\mathrm{M}}, \phi_{3\mathrm{M}})$; see Fig. 6(d). For (3.5) to be satisfied, two plateaus are involved in the intersection. A necessary condition for this is that the flux value of the local maximum of j_2 is larger than or equal to the flux value of the local minimum of j_3, i.e.,

$$j_2(\phi_2^{\mathrm{M}}) \geq j_3(\phi_{3\mathrm{M}}). \tag{FII}$$

(e) $\phi_2 \in [\phi_2^{\mathrm{M}}, \phi_{2\mathrm{M}})$, $\phi_3 \in (\phi_3^{\mathrm{M}}, \phi_{3\mathrm{M}}]$. An intersection occurs between the decreasing part of $\check{j}_2(\cdot; \phi_2)$ and the plateau of $\hat{j}_3(\cdot; \phi_3)$ only if (FII) holds. We have $q_2 \leq q_3 \Leftrightarrow \phi_2 \leq \phi_3$.

(f) $\phi_2 \in [\phi_{2\mathrm{M}}, 1]$, $\phi_3 \in (\phi_3^{\mathrm{M}}, \phi_{3\mathrm{M}}]$. Two plateaus are necessarily involved in the intersection, which occurs only if the following condition is satisfied:

$$j_2(1) \geq j_3(\phi_{3\mathrm{M}}). \tag{FIII}$$

(g) $\phi_2 \in [0, \phi_2^{\mathrm{M}}]$, $\phi_3 \in (\phi_{3\mathrm{M}}, 1]$. The intersection occurs at the flux level $j_3(\phi_{3\mathrm{M}}) = \hat{j}_3(\phi_{3\mathrm{M}}; \phi_3)$. However, $\phi_3 = \phi_{3\mathrm{M}}$ is not allowed in this subcase, so (3.5) is not satisfied and this case is therefore empty.

(h) $\phi_2 \in (\phi_2^{\mathrm{M}}, \phi_{2\mathrm{M}})$, $\phi_3 \in (\phi_{3\mathrm{M}}, 1]$. This case is empty with the same motivation as in subcase (g).

(i) $\phi_2 \in [\phi_{2\mathrm{M}}, 1]$, $\phi_3 \in [\phi_{3\mathrm{M}}, 1]$. Similarly to subcase (f), a steady-state solution is possible only if (FIII) holds. We have $q_2 \leq q_3 \Leftrightarrow \phi_2 \leq \phi_3$.

2. **Case F2.** $q_2 \leq 0 \leq q_3$. We use the same principle of subdivision as in Case F1. However, when $q_2 \leq 0$, the local minimizer of $j_2(\cdot; q_2)$ is $\phi_{2\mathrm{M}} = 1$, so the domain of $j_2(\cdot; q_2)$ consists of two disjoint intervals where j_2 is monotone. Together with the three intervals of j_3, we get six subcases.

(a) $\phi_2 \in [0, \phi_2^{\mathrm{M}}]$, $\phi_3 \in [0, \phi_3^{\mathrm{M}}]$. As can be seen in Fig. 7(a), there is always a possible intersection between $\check{j}_2(\cdot; \phi_2)$ and $\hat{j}_3(\cdot; \phi_3)$. We have either $q_2 < q_3 \Leftrightarrow \phi_3 < \phi_2$, or $q_2 = q_3 = 0 \Leftrightarrow \phi_2 = \phi_3$. This subcase is thus similar to Case F1(a).

(b) $\phi_2 \in (\phi_2^{\mathrm{M}}, 1]$, $\phi_3 \in [0, \phi_3^{\mathrm{M}}]$. This case is empty with analogous arguments as in Case F1(b).

(c) $\phi_2 \in [0, \phi_2^{\mathrm{M}}]$, $\phi_3 \in (\phi_3^{\mathrm{M}}, \phi_{3\mathrm{M}}]$. The intersection of $\check{j}_2(\cdot; \phi_2)$ and $\hat{j}_3(\cdot; \phi_3)$ is qualitatively the same as in Case F1(d) and (e) and the steady state represented in Fig. 7(c) is possible only if (FII) holds.

(d) $\phi_2 \in (\phi_2^{\mathrm{M}}, 1]$, $\phi_3 \in (\phi_3^{\mathrm{M}}, \phi_{3\mathrm{M}}]$. By analogy with subcase (c), (FII) has to be satisfied.

(e) $\phi_2 \in [0, \phi_2^{\mathrm{M}}]$, $\phi_3 \in (\phi_{3\mathrm{M}}, 1]$. This case is analogous to Case F1(g), and is consequently empty.

(f) $\phi_2 \in (\phi_2^{\mathrm{M}}, 1]$, $\phi_3 \in (\phi_{3\mathrm{M}}, 1]$. Analogous to Case F1(h) and empty case.

3. **Case F3.** $q_2 \leq q_3 \leq 0$. In this case $\phi_{2\mathrm{M}} = \phi_{3\mathrm{M}} = 1$, so there are only four subcases with the maximum point of each flux function as the point of division of two monotonicity intervals.

(a) $\phi_2 \in [0, \phi_2^{\mathrm{M}}]$, $\phi_3 \in [0, \phi_3^{\mathrm{M}}]$. This is qualitatively the same as Case F2(a) with steady-state solution possible.

(b) $\phi_2 \in (\phi_2^{\mathrm{M}}, 1]$, $\phi_3 \in [0, \phi_3^{\mathrm{M}}]$. This case is empty with analogous arguments as in Case F1(b) or F2(b) (no plot is shown).
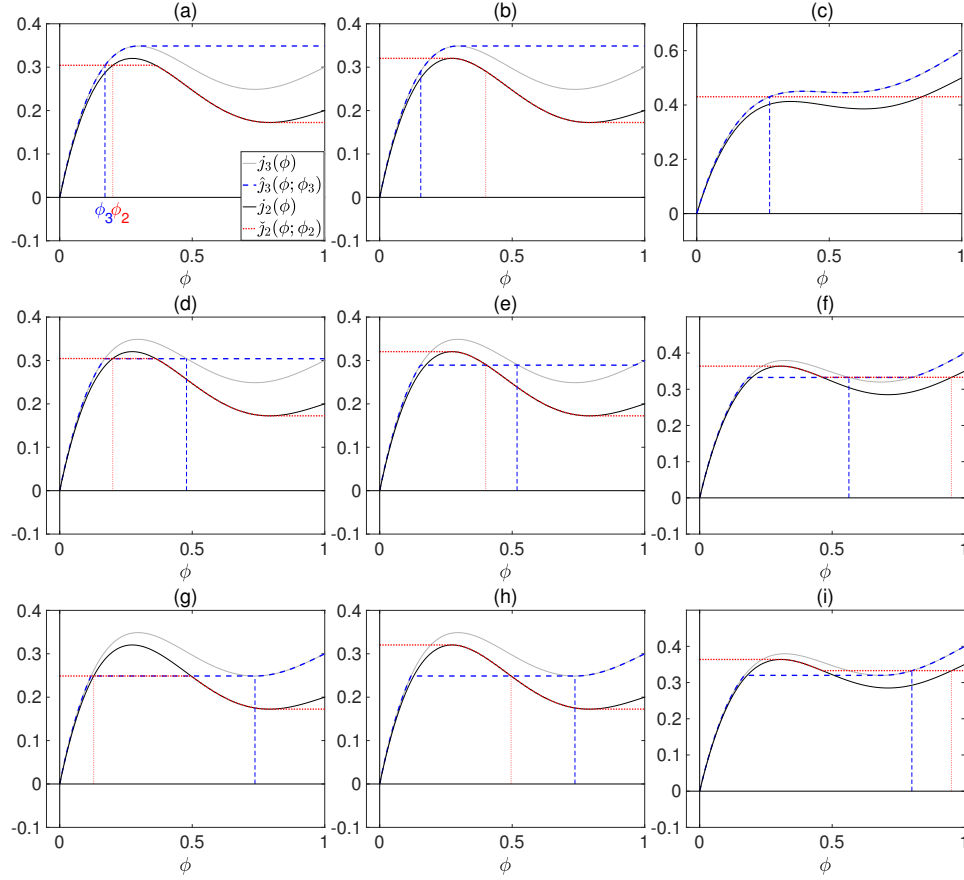
FIGURE 6. Case F1: $0 \leq q_2 \leq q_3$. Possible steady-state values for zones 2 and 3. In the special case $q_2 = q_3$, the diagonal plots (a), (e) and (i) are the only ones where $\phi_2 = \phi_3$ occurs.

(c) $\phi_2 \in [0, \phi_2^M]$, $\phi_3 \in (\phi_3^M, 1]$. There is a possible intersection only at a non-negative flux value. Then bubbles flow upwards and we have $\phi_3 \in [\phi_3^M, \phi_{3Z}]$, see Fig. 8(c).

(d) $\phi_2 \in (\phi_2^M, 1]$, $\phi_3 \in (\phi_3^M, 1]$. Intersection may occur at a positive or negative flux value (bubbles moving downwards or upwards), see Fig. 8(d1) and (d2), respectively.

3.6. **Couplings at** $z = z_W$. Since $\phi_W = 0$, the fluxes to consider for the entropy condition are $\check{\jmath}_3(\cdot; \phi_3)$ and $\hat{\jmath}_4(\cdot; \phi_4)$. From (3.4) we know that only $\phi_4 \in [0, \phi_{4m}] \cup [\phi_{4M}, 1]$ are possible steady states in zone 4. In these two intervals, j_4 is increasing and we combine these intervals with the three monotone parts of j_3.

1. **Case W1.** $0 \leq q_3 \leq q_4$.
   (a) $\phi_3 \in [0, \phi_3^M]$, $\phi_4 \in [0, \phi_{4m}]$; see Fig. 9(a).
   (b) $\phi_3 \in (\phi_3^M, \phi_{3M})$, $\phi_4 \in [0, \phi_{4m}]$ is an empty case (no plot is shown).
   (c) $\phi_3 \in [\phi_{3M}, 1]$, $\phi_4 \in [0, \phi_{4m}]$ is an empty case (no plot is shown).
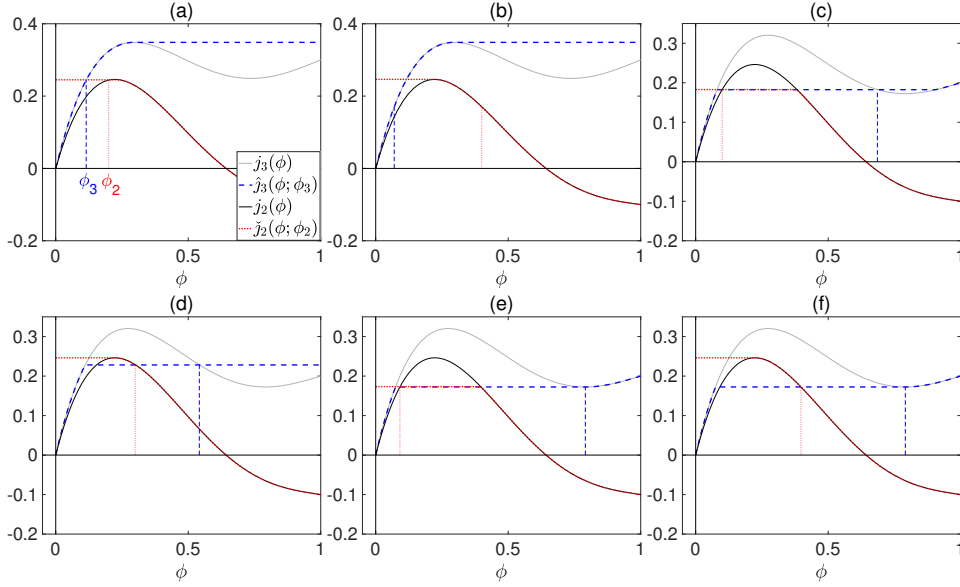
FIGURE 7. Case F2, $q_2 \leq 0 \leq q_3$: Possible intersections and steady states for zones 2 and 3.

(d) $\phi_3 \in [0, \phi_3^M]$, $\phi_4 \in [\phi_{4M}, 1]$; see Fig. 9(d). Necessarily, $\phi_4 = \phi_{4M}$ holds. Another necessary condition for this steady state is that the flux value of the local maximum of j_3 is larger than or equal to the flux value of the local minimum of j_4, i.e.,

$$j_3(\phi_3^M) \geq j_4(\phi_{4M}). \tag{WI}$$

(e) $\phi_3 \in [\phi_3^M, \phi_{3M})$, $\phi_4 \in [\phi_{4M}, 1]$; see Fig. 9(e). In this case $\phi_4 = \phi_{4M}$ and the necessary condition is (WI).

(f) $\phi_3 \in [\phi_{3M}, 1]$, $\phi_4 \in [\phi_{4M}, 1]$; see Fig. 9(f). This case is empty unless the following condition holds:

$$j_3(1) \geq j_4(\phi_{4M}). \tag{WII}$$

2. **Case W2.** $q_3 \leq 0 \leq q_4$. The conclusions are the same as in Case W1.

3.7. **Operating charts for bulk velocities.** The different necessary conditions on the fluxes that appear in the derivation of possible steady states can be visualized in operating charts. These are two-dimensional diagrams involving the bulk velocities at an injection point.

Condition (G) can be written as

$$q_G \leq j_2(\phi_2^M(q_2); q_2), \tag{G}$$

where the dependence on q_2 is written out as in Lemma 2.1. This lemma gives that $j_2(\phi_2^M(q_2); q_2)$ is an increasing function of intermediate (normal) values of q_2 and otherwise constant (for $q_2 < q_{neg}$ and $q_2 > \bar{\bar{q}}$). Its graph, and consequently the region in (q_2, q_G)-space where (G) is satisfied, are shown in Fig. 10(a). In Fig. 10(b),
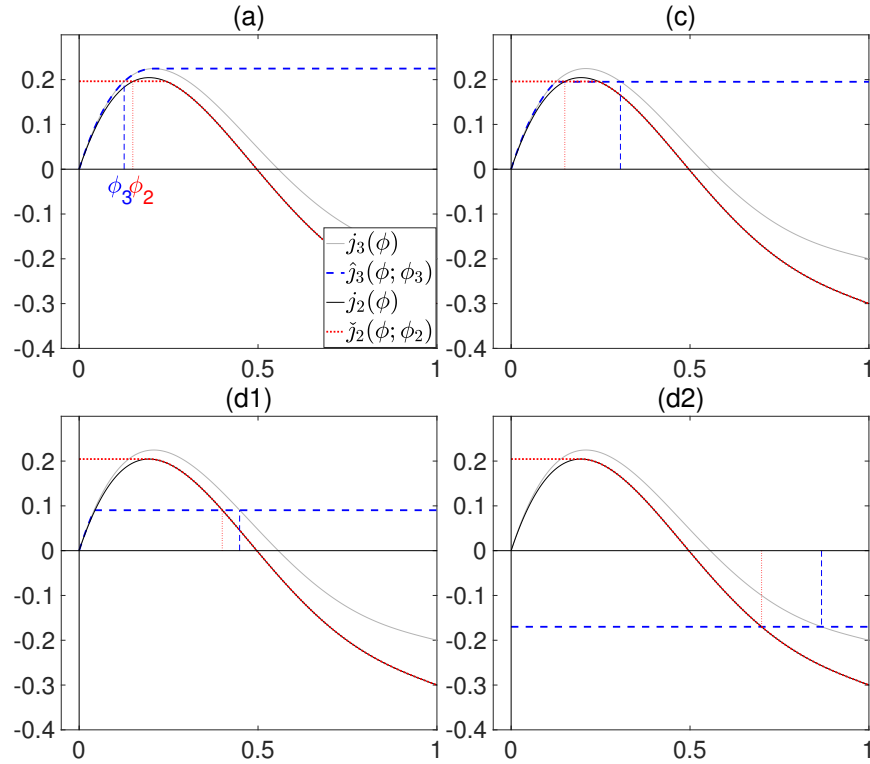
FIGURE 8. Case F3, $q_2 \leq q_3 \leq 0$. Possible intersections and steady-state values for zones 2 and 3. (d1) and (d2) correspond to positive and negative intersection flux values in subcase (d), respectively.

the corresponding region in (q_U, q_G)-space is shown. This has been obtained by the linear mapping of the curve $q_G = j_2(\phi_2^M(q_2); q_2)$ (since $q_U = q_G - q_2$):

$$\begin{cases} q_U = j_2(\phi_2^M(q_2); q_2) - q_2, \\ q_G = j_2(\phi_2^M(q_2); q_2). \end{cases}$$

We will now do same for the coupling at $z = z_F$ and conditions (FI)–(FIII). These lead to overlapping regions in the (q_2, q_3)-plane leading to different numbers of possible steady states in different regions. In Fig. 11, the regions are shadowed in which (FI) (red), (FII) (blue) and (FIII) (grey) hold.

To obtain these regions, we define the following functions with respect to conditions (FI)–(FII):

$$h_I(q_2) := j_2(1; q_2) - j_2(\phi_2^M(q_2); q_2) = q_2 - j_2(\phi_2^M(q_2); q_2),$$
$$h_{II}(q_2, q_3) := j_2(\phi_2^M(q_2); q_2) - j_3(\phi_{3M}(q_3); q_3).$$

These functions are continuously differentiable by Lemma 2.1. The following lemma gives the qualitative properties of the boundaries of the regions.
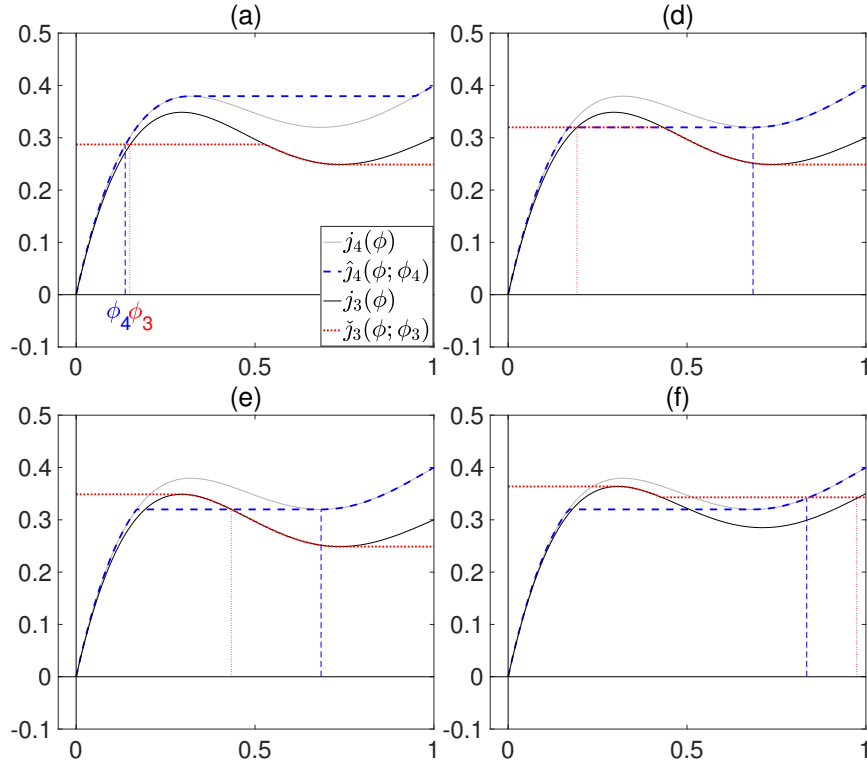
FIGURE 9. Case W1: $0 \leq q_3 \leq q_4$. Possible steady-state values for zones 3 and 4. Subcases (b) and (c) are not plotted since they are empty cases.

Lemma 3.1. *There exists a unique $\tilde{q} \in (0, \bar{\bar{q}})$ and a unique continuously differentiable function $\tilde{h}_{\mathrm{II}}$ such that $\tilde{q} = j_3(\phi_{3\mathrm{M}}(\tilde{q}); \tilde{q})$ and the following hold:*

$$\text{(FI)} \quad \Leftrightarrow \quad h_{\mathrm{I}}(q_2) \gtreqqless 0 \quad \Leftrightarrow \quad q_2 \gtreqqless \tilde{q}, \tag{3.6}$$

$$\text{(FII)} \quad \Leftrightarrow \quad h_{\mathrm{II}}(q_2, q_3) \geq 0 \quad \Leftrightarrow \quad q_3 \leq \tilde{h}_{\mathrm{II}}(q_2), \tag{3.7}$$

$$\text{(FIII)} \quad \Leftrightarrow \quad q_2 \geq j_3(\phi_{3\mathrm{M}}(q_3); q_3), \tag{3.8}$$

$$\tilde{h}_{\mathrm{II}}(q_2) = \begin{cases} 0 & \text{if } q_2 \leq q_{\mathrm{neg}}, \\ \text{increasing} & \text{if } q_{\mathrm{neg}} < q_2 < \bar{\bar{q}}, \\ q_2 & \text{if } q_2 \geq \bar{\bar{q}}, \end{cases}$$

$$j_3(\phi_{3\mathrm{M}}(q_3); q_3) = \begin{cases} q_3 & \text{if } q_3 \leq \bar{q}, \\ \text{increasing} & \text{if } \bar{q} < q_3 < \bar{\bar{q}}, \\ j_{\mathrm{g}}(\phi_{\mathrm{infl}}) + q_3 \phi_{\mathrm{infl}} & \text{if } q_3 \geq \bar{\bar{q}}. \end{cases}$$

Proof. Using Lemma 2.1, we get

$$h'_{\mathrm{I}}(q_2) = 1 - \phi_2^{\mathrm{M}} > 0,$$

$$h_{\mathrm{I}}(0) = -j_2(\phi_2^{\mathrm{M}}(0); 0) = -j_g(\phi_2^{\mathrm{M}}(0)) < 0,$$

$$h_{\mathrm{I}}(\bar{\bar{q}}) = j_2(1; \bar{\bar{q}}) - j_2(\phi_{\mathrm{infl}}; \bar{\bar{q}}) > 0,$$
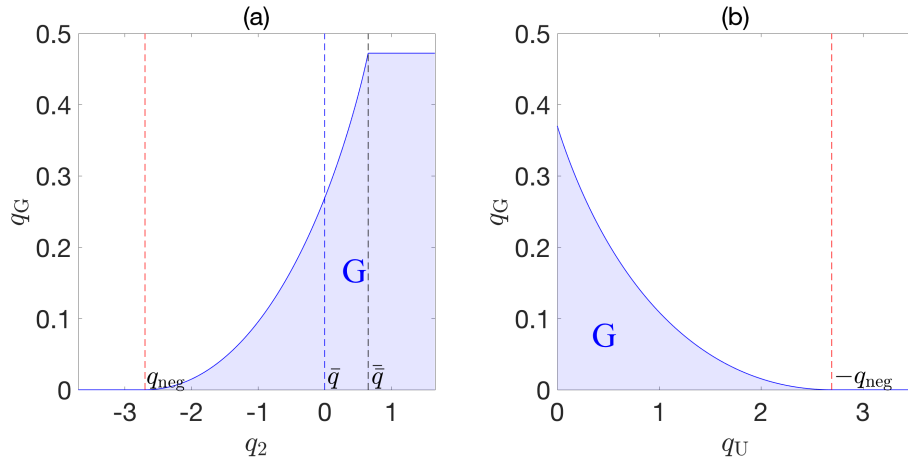
FIGURE 10. Operating charts in which condition (G) is satisfied in (a) (q_2, q_G)-plane and (b) (q_U, q_G)-plane. As usual, the unit of q-fluxes is cm/s.
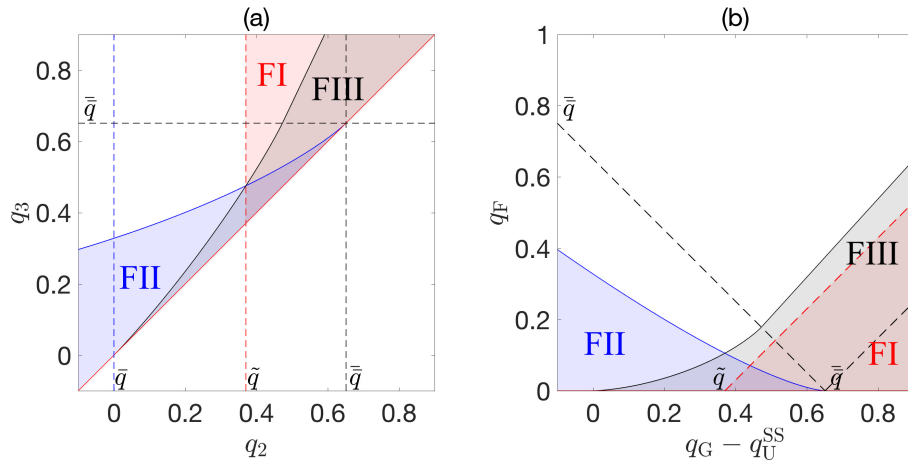

FIGURE 11. Operating charts in which conditions (FI)–(FIII) are satisfied in (a) (q_2, q_3)-plane (where $q_3 \geq q_2$ holds) and (b) (q_G, q_F)-plane. The value $q_{\text{neg}} = -2.6941\,\text{cm/s}$ is not shown in these and further plots. In the latter plot, the scale of the horizontal axis is adjusted with respect to the previously chosen fixed value q_U^{SS}.

where the last inequality follows from the fact that $j_2(\cdot; \bar{\bar{q}})$ is an increasing function. Hence, h_I is a continuous increasing function and (3.6) follows. For condition (FII), we have (by means of Lemma 2.1)

$$\frac{\partial h_{II}}{\partial q_2} = \phi_2^M(q_2) \gtreqless 0 \quad \Leftrightarrow \quad q_2 \gtreqless q_{\text{neg}},$$

$$\frac{\partial h_{\mathrm{II}}}{\partial q_3} = -\phi_{3\mathrm{M}}(q_3) < 0 \quad \text{for all } q_3.$$

Since the latter derivative is always non-zero, the implicit function theorem implies the existence of a continuously differentiable function $\tilde{h}_{\mathrm{II}}$ satisfying

$$h_{\mathrm{II}}\big(q_2; \tilde{h}_{\mathrm{II}}(q_2)\big) = 0 \quad \text{for all } q_2,$$

$$\tilde{h}'_{\mathrm{II}}(q_2) = -\frac{\partial h_{\mathrm{II}}/\partial q_2}{\partial h_{\mathrm{II}}/\partial q_3} \gtreqqless 0 \quad \Leftrightarrow \quad q_2 \gtreqqless q_{\mathrm{neg}}.$$

For $q_2 \le q_{\mathrm{neg}}$ and $q_3 = 0$, we have

$$h_{\mathrm{II}}(q_2, 0) = j_2(0; q_2) - j_3(1; 0) = 0 - 0 = 0 \quad \Rightarrow \quad \tilde{h}_{\mathrm{II}}(q_2) = 0,$$

and for $q_3 = q_2 \ge \bar{\bar{q}}$, we have

$$h_{\mathrm{II}}(q_2, q_2) = j_2(\phi_{\mathrm{infl}}; q_2) - j_3(\phi_{\mathrm{infl}}; q_2) = \phi_{\mathrm{infl}}(q_2 - q_2) = 0 \quad \Rightarrow \quad \tilde{h}_{\mathrm{II}}(q_2) = q_2,$$

Condition (FIII) can directly be rewritten by using the identity $j_2(1; q_2) = q_2$. Hence, the boundary of the region where condition (FIII) holds is given by the curve $j_3(\phi_{3\mathrm{M}}(q_3); q_3)$, and its properties follow from Lemma 2.1 and the definition of $\phi_{3\mathrm{M}}(q_3)$. Finally, the definition of $\tilde{q}$ gives that

$$j_3(\phi_3^{\mathrm{M}}(\tilde{q}); \tilde{q}) - \tilde{q} = j_2(\phi_2^{\mathrm{M}}(\tilde{q}); \tilde{q}) - \tilde{q} = h_{\mathrm{I}}(\tilde{q}) = 0.$$

$\square$

As we did for the gas injection point, we now transform the boundary curves of conditions (FI)–(FIII) from the (q_2, q_3)-plane to the $(q_{\mathrm{G}}, q_{\mathrm{F}})$-plane with the linear mapping

$$\begin{cases} q_{\mathrm{G}} = q_{\mathrm{U}}^{\mathrm{SS}} + q_2, \\ q_{\mathrm{F}} = q_3 - q_2. \end{cases} \quad \Leftrightarrow \quad \begin{cases} q_{\mathrm{G}} - q_{\mathrm{U}}^{\mathrm{SS}} = q_2, \\ q_{\mathrm{F}} = q_3 - q_2. \end{cases}$$

This mapping depends on the chosen steady-state value of q_{U}, denoted by $q_{\mathrm{U}}^{\mathrm{SS}}$, from the chart in Fig. 10(b). For a given value of $q_{\mathrm{U}}^{\mathrm{SS}}$, we therefore use the scale $q_{\mathrm{G}} - q_{\mathrm{U}}^{\mathrm{SS}}$ on the horizontal axis; see Fig. 11(b).

For the coupling at $z = z_{\mathrm{W}}$, we note that conditions (WI) and (WII) are the same as conditions (FII) and (FIII) except for the zone index increased by one. Hence, the analogous statements of Lemma 3.1 hold, except for those involving $\tilde{q}$. We can draw the operating chart in the (q_3, q_4)-plane, and with the mapping

$$\begin{cases} q_{\mathrm{F}} = q_{\mathrm{U}}^{\mathrm{SS}} - q_{\mathrm{G}}^{\mathrm{SS}} + q_3, \\ q_{\mathrm{W}} = q_4 - q_3, \end{cases} \quad \Leftrightarrow \quad \begin{cases} q_{\mathrm{F}} - (q_{\mathrm{U}}^{\mathrm{SS}} - q_{\mathrm{G}}^{\mathrm{SS}}) = q_3, \\ q_{\mathrm{W}} = q_4 - q_3, \end{cases}$$

the chart in the $(q_{\mathrm{F}}, q_{\mathrm{W}})$-plane, where the steady-state values $q_{\mathrm{U}}^{\mathrm{SS}}$ and $q_{\mathrm{G}}^{\mathrm{SS}}$ have been chosen from the previous operating charts; see Fig. 12.

It seems logical that when working with steady states, it is necessary to restrict the amount of gas, fluid or water pumped into the tank. Moreover, from the desliming point of view, situations as huge quantities of fluid leaving at the top of the column, loosening the froth or washing it in excess, or gas bubbles flowing down and out of the tank through the bottom tailings underflow, are not convenient. Conditions (G), (FI)–(FIII) and (WI)–(WII) set a theoretical upper limit for the values of q_{G}, q_{F} and q_{W}, respectively, for a fixed given value of $q_{\mathrm{U}}^{\mathrm{SS}}$, as Figures 10–12 show. For instance, Fig. 11(b) shows that if we want any condition (FI)–(FIII) to be satisfied for $q_{\mathrm{G}} - q_{\mathrm{U}}^{\mathrm{SS}} \in [-0.1, 0.9]\,\mathrm{cm/s}$, then we should set $q_{\mathrm{F}} < 0.7\,\mathrm{cm/s}$.
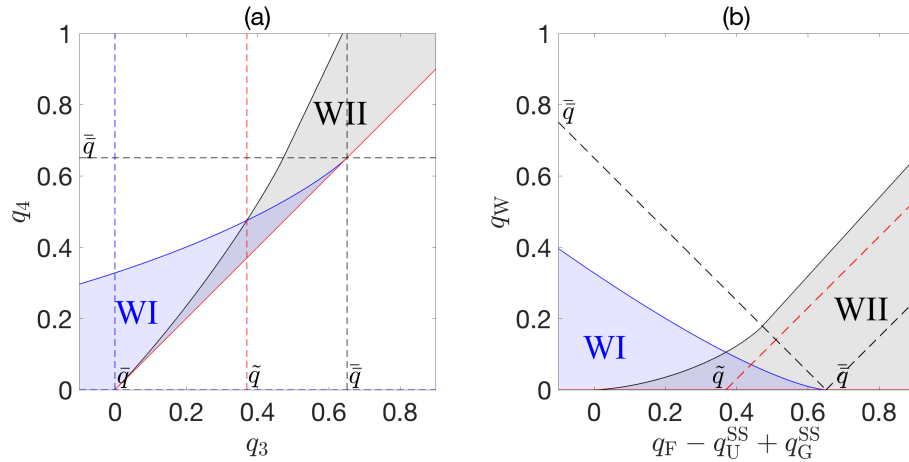
FIGURE 12. Operating charts in which conditions (WI)–(WII) are satisfied in (a) (q_3, q_4)-plane and (b) (q_F, q_W)-plane. In the latter plot, the scale of the horizontal axis is adjusted with respect to the previously chosen fixed values q_U^{SS} and q_G^{SS}.

3.8. Tables and visualization of steady states.

Whereas the operating charts in Section 3.7 give an overview on how to choose the bulk velocities with respect to conditions for certain steady-state couplings at the points of injection and outlets, we here collect in Tables 1 and 3 all possible steady-state combinations between these couplings for the cases $q_3 \geq q_2 \geq 0$ and $q_2 < 0$, respectively. Some of the couplings made locally, for example for ϕ_2 and ϕ_3 in Section 3.5, do not appear in the tables because they are not possible when taking into account also the couplings with ϕ_1 and ϕ_4.

The tables should be read as follows. A possible steady-state solution with constant concentration in each zone is obtained by connecting adjacent rectangles passing only over vertical lines (and no corners), from the left column ϕ_U to the right ϕ_E. In Table 2 we show some examples of admissible and inadmissible paths, in green and red respectively, for steady states for the case $q_3 \geq q_2 \geq 0$ in Table 1. As it can be seen, the inadmissible path passes over a horizontal line in the ϕ_2-column, yielding two different possible intervals of definition for ϕ_2, which is not allowed.

Table 3 shows the possible steady states when $q_2 < 0$ and the sign restrictions of q_3 are given in the table. The appearance of conditions (G), (FI), etc. in the tables means that the corresponding steady state is possible only if the corresponding conditions are satisfied. As can be seen in the first and the last columns of the tables, the values of ϕ_U and ϕ_E are uniquely given by the chosen value of ϕ_1 and ϕ_4, respectively. Also notice that although in the derivation of the cases we allow the intervals of definition of ϕ_i to overlap, we do not do this in the construction of the tables, to avoid the appearance of a possible steady state more than once and keep the tables as simple as possible.

3.9. Steady states having discontinuities within zones.

Despite the diversity of possible steady states with a constant value in each zone, which are categorized

ϕ_U	ϕ_1	ϕ_2	ϕ_3	ϕ_4	ϕ_E
	0 (G)	$[0, \phi_2^M]^*$	$[0, \phi_3^M]$	$[0, \phi_{4m}]$	
	$[\phi_{1Z}, 1]$				
	0 (G)	$(\phi_2^M, \phi_{2M}]$	$(\phi_3^M, \phi_{3M}]$ (FII)	ϕ_{4M} (WI)	
$-\dfrac{j_1(\phi_1)}{q_U}$	$[\phi_{1Z}, 1]$				$\dfrac{j_4(\phi_4)}{q_E}$
	0 ($q_1 = 0$)	1	$[0, \phi_3^M]$ (FI)	$[0, \phi_{4m}]$	
			$(\phi_3^M, \phi_{3M}]$ (FIII)	ϕ_{4M} (WI)	
	1		$[\phi_{3M}, 1]$ (FIII)	ϕ_{4M} (WII)	

TABLE 1. Collection of possible steady states for the flotation column when $q_2 = q_G - q_U \geq 0$. $^{(*)}$When $\phi_1 \in [\phi_{1Z}, 1]$ then $\phi_2 = \phi_2^M$.
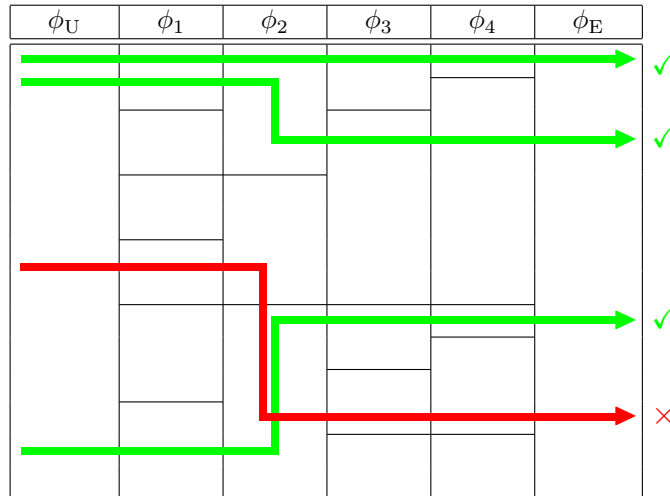
TABLE 2. Admissible (green) and inadmissible (red) paths for steady-state construction in Table 1.

in Tables 1 and 3, there exist further steady states with possible stationary discontinuities within the zones. For example, in zone 1, the constant solutions $\phi_1 = 0$ and ϕ_{1Z} have the same flux value, i.e., $j_1(0) = j_1(\phi_{1Z})$. This means that there may be a stationary discontinuity from $\phi_1 = 0$ below to ϕ_{1Z} above the discontinuity, which may be located anywhere in the interval (z_U, z_G), since the entropy condition (2.9) is satisfied. If such a discontinuity exists in zone 1, then the value ϕ_{1Z} can be coupled with admissible values of ϕ_2 according to Table 1 or 3.

ϕ_{U}	ϕ_1	ϕ_2	ϕ_3	ϕ_4	ϕ_{E}
$-\dfrac{j_1(\phi_1)}{q_{\mathrm{U}}}$	0 (G)	$[0,\phi_2^{\mathrm{M}}]^*$	$[0,\phi_3^{\mathrm{M}}]$	$[0,\phi_{4\mathrm{m}}]$	$\dfrac{j_4(\phi_4)}{q_{\mathrm{E}}}$
			$(\phi_3^{\mathrm{M}},\phi_{3\mathrm{M}}]$ (FII) $q_3 \geq 0$		
	$[\phi_{1\mathrm{Z}},1]$		$(\phi_3^{\mathrm{M}},\phi_{3\mathrm{Z}}]$ $q_3 \leq 0$	$\phi_{4\mathrm{M}}$ (WI)	
	0 (G)	$(\phi_2^{\mathrm{M}},\phi_{2\mathrm{Z}}]$	$(\phi_3^{\mathrm{M}},\phi_{3\mathrm{M}}]$ (FII) $q_3 \geq 0$		
	$[\phi_{1\mathrm{Z}},1]$		$(\phi_3^{\mathrm{M}},\phi_{3\mathrm{Z}}]$ $q_3 \leq 0$		

TABLE 3. Collection of possible steady-states for the flotation column when $q_2 = q_{\mathrm{G}} - q_{\mathrm{U}} < 0$. $^{(*)}$When $\phi_1 \in [\phi_{1\mathrm{Z}},1]$ then $\phi_2 = \phi_2^{\mathrm{M}}$.

In the same way, stationary discontinuities from a lower to a higher value are possible in zones 2, 3 and 4 for all bulk velocities q_k that imply that the drift-flux function in the zone is not monotone; hence, $q_k > q_{\mathrm{neg}}$ should hold. Analogously, there may be discontinuities from higher gas volume fraction below a standing discontinuity than above, if the drift flux has its local minimum point $\phi_{k\mathrm{M}}(q_k) \in (\phi_{\mathrm{infl}}, 1)$, which is equivalent to $q_k \in (\bar{q}, \bar{\bar{q}})$. We provide examples of such discontinuities in Section 5.

4. **Numerical method.** For the discretization of the model, we follow the procedure of [3] for the sedimentation process in a clarifier-thickener.

We subdivide the tank into N internal layers, or cells, and four external layers, two at the top and two at the bottom, corresponding to the overflow and underflow zones, respectively, each of them with depth $\Delta z = 1/N$. We let $\phi^i(t) \approx \phi(z_i, t)$ denote the average of the exact solution over layer i, i.e. (z_{i-1}, z_i), at time t, i.e.,

$$\phi^i(t) := \frac{1}{\Delta z} \int_{z_{i-1}}^{z_i} \phi(z,t)\, \mathrm{d}z.$$

For each layer i, we use the balance law corresponding to (1.1) to obtain

$$\frac{\mathrm{d}\phi^i}{\mathrm{d}t} = -\frac{F(z_i,t,\phi^i) - F(z_{i-1},t,\phi^{i-1})}{\Delta z} + \frac{1}{\Delta z} \sum_{S \in \{\mathrm{G,F,W}\}} \int_{z_{i-1}}^{z_i} q_S \phi_S \delta(z - z_S)\, \mathrm{d}z,$$
(4.1)

where the flux $F(z,t,\phi)$ is defined by (2.7). This is approximated by Godunov's numerical flux [23], which is

$$\mathcal{F}_i := \mathcal{F}_i(\phi^i, \phi^{i+1}, t) = \begin{cases} \min\limits_{\phi^i \leq \phi \leq \phi^{i+1}} j_k(\phi) & \text{if } \phi^i \leq \phi^{i+1}, \\ \max\limits_{\phi^i \geq \phi \geq \phi^{i+1}} j_k(\phi) & \text{if } \phi^i > \phi^{i+1}, \end{cases}$$
(4.2)

where $k \in \{E, 1, 2, 3, 4, U\}$ denotes the present zone of the vessel (k depends on i). We define the indices i_G, i_F, i_W to indicate that the gas inlet is located in the layer (z_{i_G-1}, z_{i_G}), and the fluid and wash water inlets in (z_{i_F-1}, z_{i_F}) and (z_{i_W-1}, z_{i_W}), respectively. For instance, the numerical fluxes $\mathcal{F}_i$ between layers (z_{i_G-1}, z_{i_G}) and (z_{i_F-1}, z_{i_F}) will be computed using the function $j_2(\phi)$.

Substituting the numerical fluxes into the exact version of the conservation law (4.1), we get the following method-of-lines formula:

$$\frac{\mathrm{d}\phi^i}{\mathrm{d}t} = -\frac{\mathcal{F}_i - \mathcal{F}_{i-1}}{\Delta z} + \sum_{S \in \{W, F, G\}} \frac{q_S \phi_S}{\Delta z} \delta_{i,i_S}, \tag{4.3}$$

where $\delta_{i,i_S} = 1$ if $i = i_S$ and 0 otherwise. Since we utilize the Godunov flux, the following is valid. For given piecewise constant (in each cell) initial data at $t = 0$, equation (4.3) is in fact exact for the cell average of the solution of PDE (1.1) for small times until any wave from a cell boundary hits another cell boundary.

Using an explicit Euler step for the approximation of the time derivative and the CFL condition

$$\Delta t \max_{k \in \{U, 1, 2, 3, 4, E\}} \left(\max_{0 \le \phi \le 1} |j'_k(\phi)| + |q_k| \right) \le \Delta z, \tag{4.4}$$

we obtain the following fully discrete method for $\phi^{i,n} \approx \phi^i(t_n)$, where the upper index n stands for evaluation at time $t = t_n$:

$$\phi^{i,n+1} = \phi^{i,n} + \frac{\Delta t}{\Delta z} \left[-\mathcal{F}_i^n + \mathcal{F}_{i-1}^n + \sum_{S \in \{W, F, G\}} q_S^n \phi_S^n \delta_{i,i_S} \right], \quad i = -1, \ldots, N+2.$$

5. **Numerical examples.** The examples demonstrate the dynamic and steady-state behaviour of a flotation column and we use dimensionless numbers. The drift-flux function $j_g(\phi) = v_{\text{term}}\phi(1-\phi)^{3.2}$ has been applied. We chose $v_{\text{term}} = 2.7\,\text{cm/s}$ in agreement with [13]. Furthermore, the height of the vessel is $100\,\text{cm}$ and we have placed the injection points equidistantly: $z_G = 25\,\text{cm}$, $z_F = 50\,\text{cm}$ and $z_W = 75\,\text{cm}$. From now on the following units are used: $q\,[\text{cm/s}]$, $z\,[\text{cm}]$ and $t\,[\text{s}]$.

5.1. **Examples 1 and 2: Transition between steady states.** First, we define an initial set of velocities for the inlets and the outlets. In order to maximize the number of possible steady states, and also satisfying conditions (G), (FII), (FIII), (WI) and (WII), we use the operating charts in Figures 10–12 to first choose $q_U = 0.1$ and $q_G = 0.2$, and then $q_F = 0.1$ and $q_W = 0.0353$, which satisfy $j_1(\phi_1) + q_G = j_4(\phi_{4M})$. With these values, the velocities in the column are

$$q(z,t) = \begin{cases} q_1 = -0.1 & \text{for } z < z_G, \\ q_2 = 0.1 & \text{for } z_G \le z < z_F, \\ q_3 = 0.2 & \text{for } z_F \le z < z_W, \\ q_4 = 0.2353 & \text{for } z \ge z_W, \end{cases}$$

and hence $q_U = q_1 = -0.1$ and $q_E = q_4 = 0.2353$. Using Table 1 we know that, for these values satisfying conditions (G), (FII), (FIII), (WI) and (WII), there are eight possible steady states with a constant volume fraction in each zone. In Table 4, the admissible paths for the case $\phi_1 = 0$ can be seen, corresponding to steady states (a)–(d) in Figure 13. The paths with $\phi_1 \in [\phi_{1Z}, 1]$ can be obtained analogously, starting from the corresponding rectangle in Table 1. A detailed description of all steady states is provided by Figures 13–15.

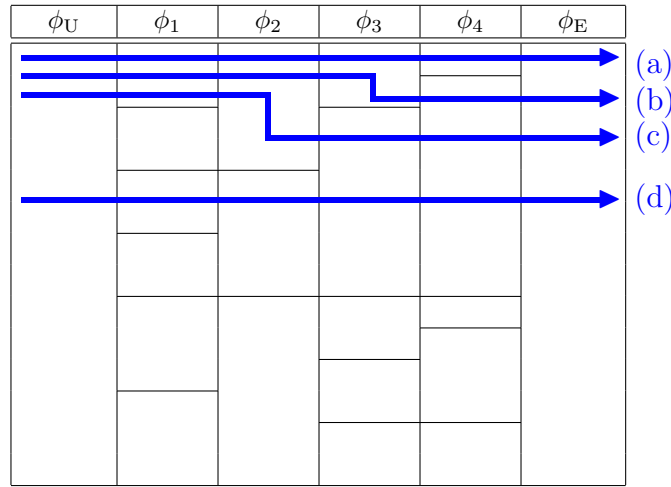| ϕ_U	ϕ_1	ϕ_2	ϕ_3	ϕ_4	ϕ_E	
						(a)
						(b)
						(c)
						(d)

TABLE 4. Examples 1 and 2: admissible paths for steady states with $\phi_1 = 0$, corresponding to steady states (a)–(d) in Figure 13.
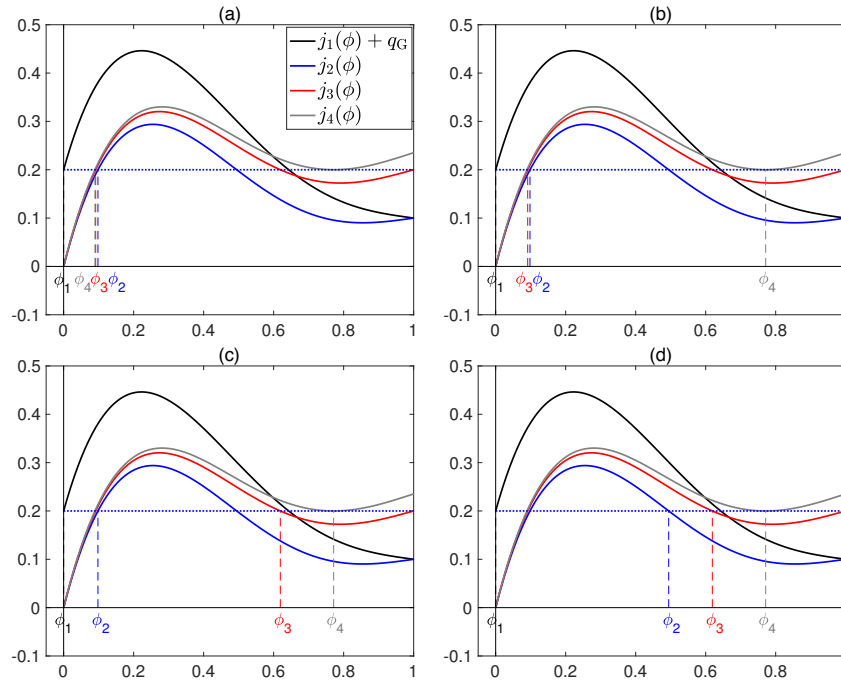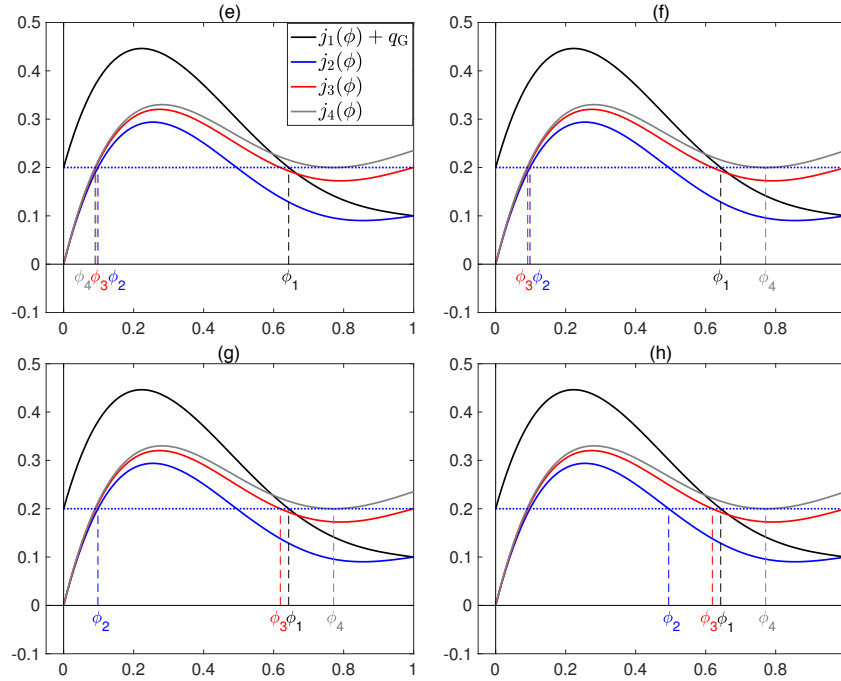

FIGURE 13. Examples 1 and 2: possible steady states with $\phi_1 = 0$ for initial data corresponding to Figures 15(a)–(d).

In addition to the volume fractions ϕ_k, $k \in \{U, 1, 2, 3, 4, E\}$, Figure 15 shows the gas and fluid fluxes (j_k and φ_k) in each zone k represented by red and blue arrows, respectively. In all eight cases, the gas flux is zero below $z = z_G$, since $j_1(\phi_1) = 0$,

FIGURE 14. Examples 1 and 2: Possible steady states with $\phi_1 \in [\phi_{1Z}, 1]$ for initial data corresponding to Figures 15(e)–(h).

and equal to the constant value $j_4(\phi_{4M})$ above. The flux of water in zone k is then $\varphi_k = q_k - j_k(\phi_k)$.

Let us now run two simulations.

Example 1. Initially, we consider a column filled with only fluid, i.e., $\phi(z, 0) = 0$ for all z, and we start pumping gas, fluid and wash water into it, with the velocities stated above. The gas rises fast and reaches the top of the vessel in a short time; see Figure 16, which shows the time evolution of the gas concentration. As can be seen in Figure 17(a), at $t = 150$, the first steady state, see Figure 15(a), has been reached. Then we close the top of the vessel by setting $q_E = 0$ and $q_U = -0.3353$ and let the gas accumulate at the top until $t = 300$, see Figure 17(b), when we open the top again (the previous values are used). As can be seen in Figures 17(c) and (d), after opening the top, a discontinuity arises within zone 3 between the fluid and wash water inlets, and becomes stationary at $z \approx 55$; see the explanation in Section 3.9. The new steady state is thus not among the eight ones shown in Figure 15, but can be seen as combination of cases (b) and (c) of both Figures 13 and 15.

Example 2. Figures 18 and 19 show the results when we close the top of the tank for a longer period, in this case until $t = 400$. Then, still another steady state is reached, namely the intermediate one of Figure 15(d) and (h) having a discontinuity in zone 1. The flux of gas is zero in zone 1, which means that there is a region of bubbles standing still with the concentration $\phi \approx 0.65$ just below the gas inlet $z_G = 25$.
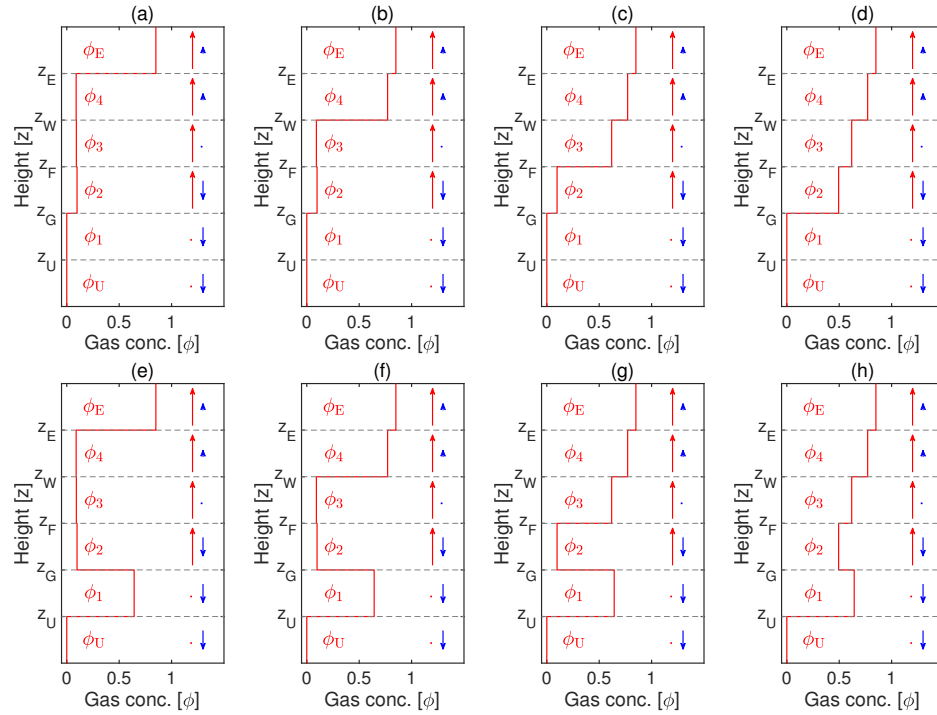
FIGURE 15. Examples 1 and 2: possible steady states with gas (red) and fluid (blue) fluxes.
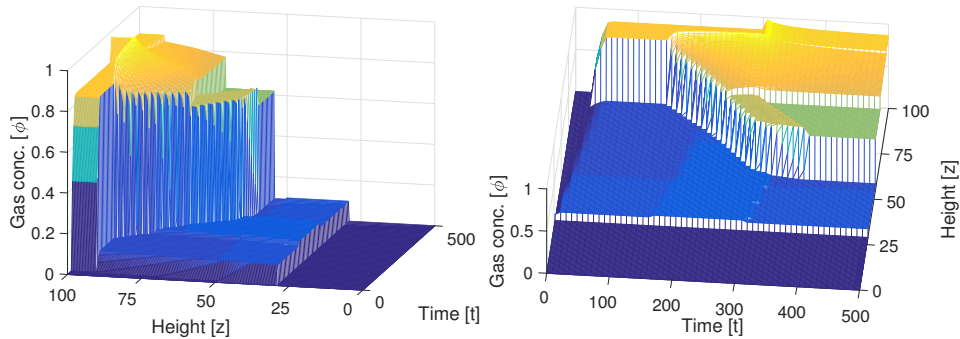

FIGURE 16. Example 1: time evolution of gas concentration from different angles.

5.2. **Example 3: Overloaded tank.** We now define an initial set of velocities for the inlets and the outlets for which no steady state with $\phi_1 = 0$ is possible. Consequently, the system is overloaded and gas has to leave also through the underflow, so that $\phi_1 > 0$. The velocities in the column chosen are
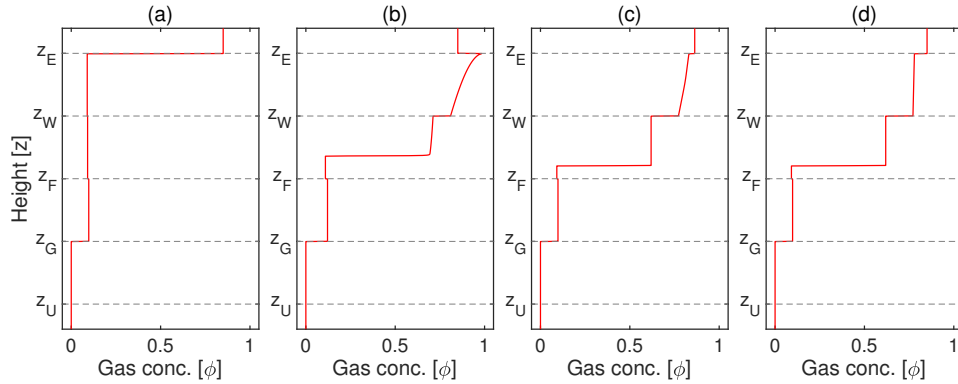
FIGURE 17. Example 1: gas concentration profiles for (a) $t = 150$, (b) $t = 300$, (c) $t = 500$ and (d) $t = 2000$.
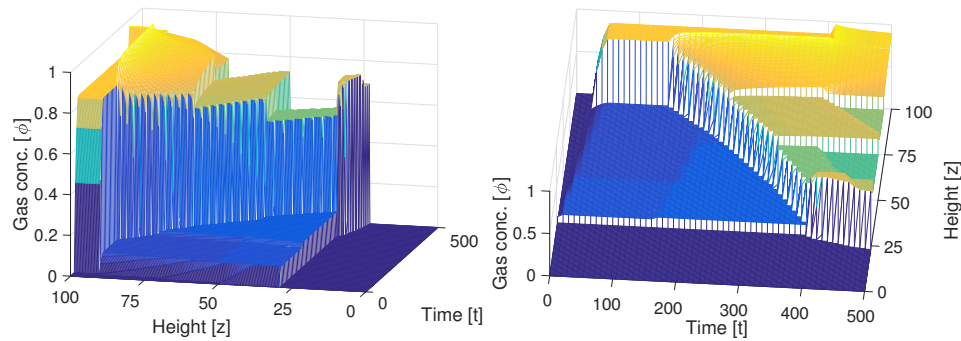
FIGURE 18. Example 2: time evolution of gas concentration from different angles.

$$q(z, t) = \begin{cases} q_1 = -0.1 & \text{for } z < z_{\text{G}}, \\ q_2 = 0.1 & \text{for } z_{\text{G}} \leq z < z_{\text{F}}, \\ q_3 = 0.15 & \text{for } z_{\text{F}} \leq z < z_{\text{W}}, \\ q_4 = 0.17 & \text{for } z \geq z_{\text{W}}, \end{cases}$$

and hence $q_{\text{U}} = q_1 = -0.1$ and $q_{\text{E}} = q_4 = 0.17$. A detailed description of the possible steady states is provided by Figure 20.

As in Examples 1 and 2, we start with a column filled with only fluid, i.e., $\phi(z, 0) = 0$ for all z, and we start pumping gas, fluid and wash water into it, with the velocities stated above. In Figure 21, we can see how the gas rises and reaches the top of the column in a short time. A steady state, corresponding to case (d) in Figure 20, has been reached by $t = 2000$, as it can be seen in Figure 21(d). Clearly this is not an acceptable set of parameters for the desliming process: an unnecessary excess of gas is flowing downwards and leaving the tank through the bottom.
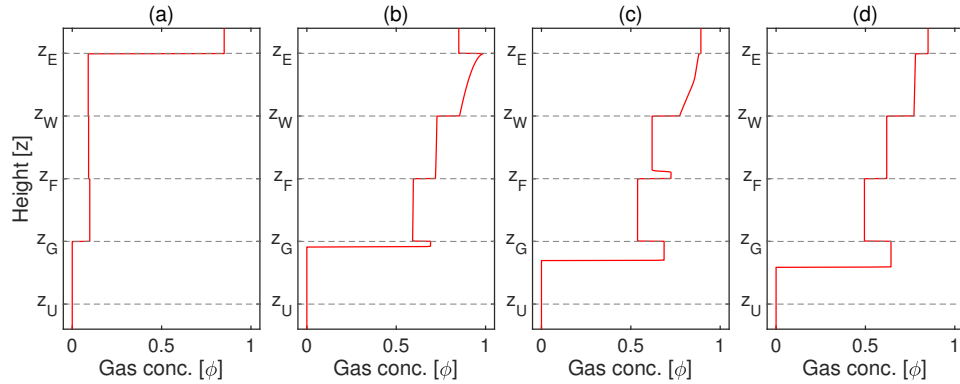
FIGURE 19. Example 2: gas concentration profiles for (a) $t = 150$, (b) $t = 400$, (c) $t = 500$ and (d) $t = 2000$.
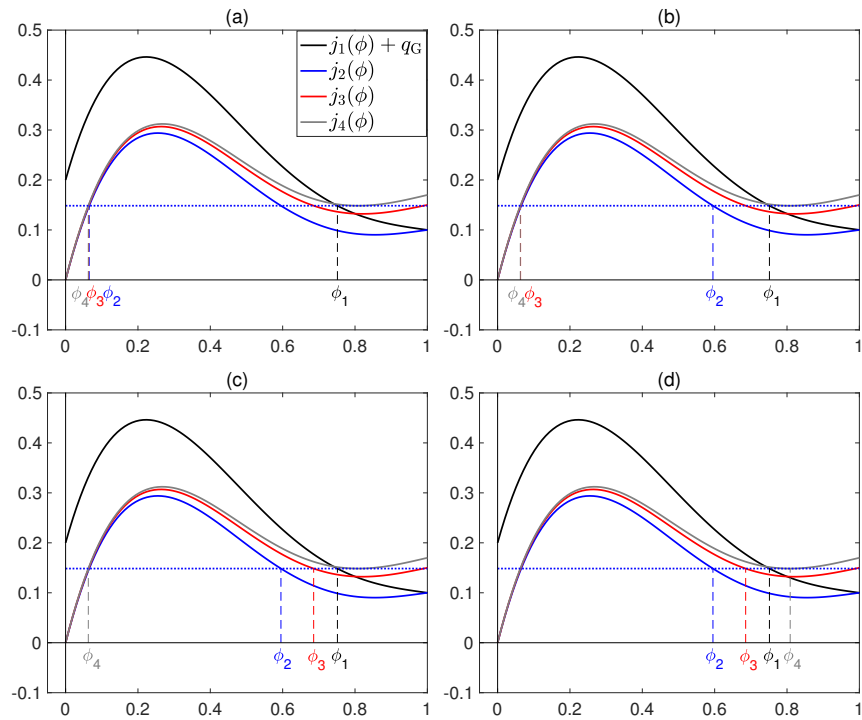

FIGURE 20. Example 3: possible steady states for initial data in Example 3.

5.3. **Example 4: Desliming.** A flotation column is generally operated so that there are two regions: one with bubbles (intermediate gas volume fraction) and one with froth. In the bubbly region, usually in zone 2 and sometimes the lower part of zone 3, the hydrophobic particles of the pulp slurry attach to the air bubbles. In the froth region, located above the bubbly region, further enrichment takes place and the foam is efficient for promoting water rejection. The injection of wash water
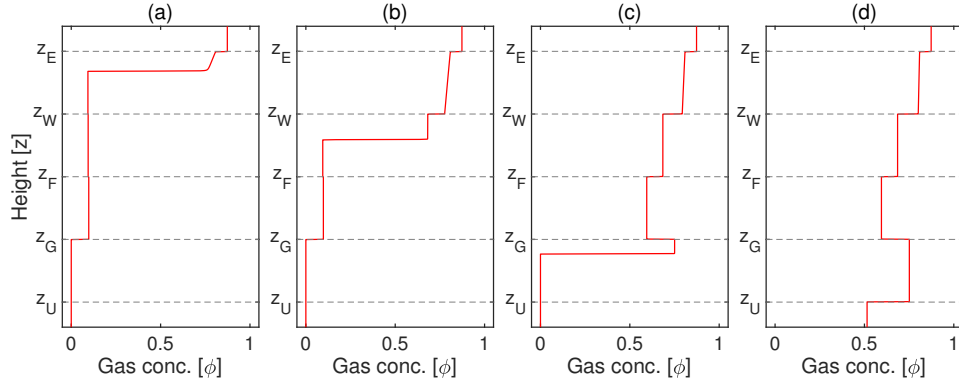
FIGURE 21. Example 3: gas concentration profiles for (a) $t = 150$, (b) $t = 500$, (c) $t = 1000$ and (d) $t = 2000$.

into the foam assists with rejection of entrained slimes. This is, however, effective only if the wash water flows downwards through the foam and bubbly regions, as stated by Dickinson and Galvin in [13]. Then the the foam is washed properly. In all steady states of Experiment 1, the wash water flows upwards.

To achieve a proper wash, the flux of water in zone 3, and consequently in zones 1 and 2, should be negative, while in zone 4, it should remain relatively small. We set $q_U = 0.11$ and $q_G = 0.1$, and choose $q_F = 0.05$ and $q_W = 0.0714$, satisfying $j_1(\phi_1) + q_G = j_4(\phi_{4M})$ to ensure that the steady state with the higher concentration of bubbles in zone 4, and hence the most ideal scenario for desliming, can be achieved. With these values, the average bulk velocities in the vessel are the following:

$$q(z,t) = \begin{cases} q_1 = -0.11 & \text{for } z < z_G, \\ q_2 = -0.01 & \text{for } z_G \leq z < z_F, \\ q_3 = 0.04 & \text{for } z_F \leq z < z_W, \\ q_4 = 0.1114 & \text{for } z \geq z_W, \end{cases}$$

hence $q_U = -0.11$ and $q_E = 0.1114$. The bulk velocity in zone 2 is negative and relatively small compared with the velocity in zone 1. Figure 22 shows the steady state with maximum concentration of gas in zones 2, 3 and 4 for the conditions given, along with the gas and water fluxes in each zone. Despite the bulk velocity in zone 3 is positive, most of the wash water injected at $z = z_W$ flows downwards through zone 3, with $\varphi_3 = -0.06$, while the flux of fluid flowing up in zone 4 and the effluent zone remains small, $\varphi_4 = 0.0114$, compared with the flux of fluid in other zones.

6. **Conclusions.** The present work has shown how the available drift-flux theory for flotation columns, to the authors' knowledge so far utilized in the engineering literature for stationary analyses only, can be combined with results coming from the mathematical and numerical analysis of conservation laws with discontinuous flux to obtain a model for transient simulations as well as prediction of steady states.

The well-posedness established in [10] for the problem of continuous sedimentation, which has one flux discontinuity, covers the case here with flotation with
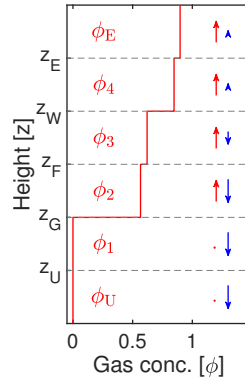
FIGURE 22. Example 4: Steady state with gas (red) and fluid (blue) fluxes for a desliming test.

several (but finite number of) discontinuities. In [10], a Kružkov-type of entropy condition was used together with a crossing condition for the fluxes for the proof of uniqueness. It is worth noting that the flux discontinuities within the present model do satisfy this condition. The entropy condition used here implies, however, the Kružkov-type and uniqueness is obtained without the crossing condition [18].

One-dimensional models such as the one treated herein are easier to solve than multi-dimensional multiphase flow models, and may be useful to model a flotation cell within plant-wide simulators [2]. Nevertheless, for practical use, the present model should be improved and refined in future work. Some suggested directions of future work are as follows. Starting with a property of the model in its present formulation, we recall that the present analysis is limited to drift flux functions j_g that satisfy (2.10), i.e., that have a horizontal tangent at $\phi = 1$, for which the Richardson-Zaki expression (2.3), (2.4) is the most common example. Results of the steady-state analysis will be more complicated, but can be obtained by similar techniques to those of Section 3, whenever $\bar{q} = -j_\mathrm{g}'(1) > 0$. To underline that this case is relevant for investigation we mention that Pal and Masliyah [31] come to the conclusion that the Richardson-Zaki expression (2.4), with $\bar{q} = 0$, is suitable with $n_\mathrm{RZ} = 2.39$. However, their Figures 10 and 11, displaying drift flux data obtained by their own experiments and from the literature, including those obtained within the froth region, strongly indicate that a function j_g with $\bar{q} > 0$ is more suitable. In fact, in their next paper [32] they modify the expression for V to $V(\phi) = 0.8(1 - \phi)\exp(-2.9\phi^{2.1})$, such that indeed $-j_\mathrm{g}'(1) = 0.8\exp(-2.9) > 0$.

With respect to the hydrodynamical setup of the flotation column and its conceptual counterpart as drawn in Figure 1, we mention that Vandenberghe et al. [39] propose an interesting recirculation: according to their Figure 1, mixture is sucked from the column at a determined level, aerated, and re-injected at another position. The extraction of material at a given rate but whose composition is part of the solution gives rise to a singular sink term whose mathematical treatment is more involved than that of a singular source term (as those appearing in (1.1)). The basic difficulty is that the sink term cannot be incorporated into the flux function; rather, the sink is represented by a new non-conservative transport term (see [6]).

In several instances, our analyses invoke available mathematical and numerical results for clarifier-thickener models. If sediment compressibility is included in a

clarifier-thickener model, an effect that arises if the solid-liquid suspension is floccu-
lated, then the governing equation for such models features an additional strongly
degenerating diffusion term [10] whose appropriate treatment, roughly speaking,
arises from handling it as part of the convective flux. Such a term may also be mo-
tivated in the application to flotation in future works: for instance, Narsimhan [29]
derives such a term to account for gradual compressibility of the foam layer that
is caused by flow of liquid through a network of plateau borders due to gravita-
tional and capillary forces [29]. On the other hand, Stevenson et al. [37] propose a
convection-diffusion model for the transport of gangue in flotation froth.

Clearly, an obvious shortcoming of the present description, although it is in line
with the cited treatments of literature [13, 22, 25, 27, 31, 32, 38, 39, 43, 44], is that it
does not explicitly model the transport and settling of solid particles. It would be
highly desirable to extend the model by solids phases, for example of hydrophobic
and hydrophilic particles (of minerals and gangue material), and to include their
attachment to bubble and transport via the liquid and gas components. The likely
outcome of such a description is a convection-diffusion-reaction system with discon-
tinuous flux akin to a recently advanced model of continuous sedimentation with
reactions [4]. On the other hand, several gas or solid phases representing size classes
that segregate and form areas of different composition can be included, and lead to
first-order hyperbolic systems of conservation laws with discontinuous flux, under
determined circumstances (see, e.g., [11] and the references cited in that paper).

Within the present work the emphasis has been on the construction of stationary
solutions. The numerical scheme utilized, Godunov's scheme with suitable modi-
fications to handle the flux discontinuities (see Section 4), is monotone provided
that Δt and Δz satisfy the CFL condition (4.4), and therefore delivers approxi-
mate solutions that converge to the unique entropy solution of the problem (1.1),
(1.2). However, formally second-order accurate solvers are possible for instance by
techniques of variable extrapolation, see e.g. [7, 9].

REFERENCES

[1] B. Andreianov, K. H. Karlsen and N. H. Risebro, A theory of L^1-dissipative solvers for scalar
conservation laws with discontinuous flux, *Arch. Rational Mech. Anal.*, **201** (2011), 27–86.

[2] O. A. Bascur, Example of a dynamic flotation framework, In: *Centenary of Flotation Sym-
posium*, Brisbane, QLD, 6–9 June 2005, Australasian Institute of Mining and Metallurgy
Publication Series, 2005, 85–91.

[3] R. Bürger, S. Diehl, S. Farås, I. Nopens and E. Torfs, A consistent modelling methodology
for secondary settling tanks: A reliable numerical method, *Water Sci. Technol.*, **68** (2013),
192–208.

[4] R. Bürger, S. Diehl and C. Mejías, A difference scheme for a degenerating convection-diffusion-
reaction system modelling continuous sedimentation, *ESAIM: Math. Model. Numer. Anal.*,
to appear.

[5] R. Bürger and K. H. Karlsen, Conservation laws with discontinuous flux: A short introduction,
J. Eng. Math., **60** (2008), 241–247.

[6] R. Bürger, A. García, K. H. Karlsen and J. D. Towers, On an extended clarifier-thickener
model with singular source and sink terms, *Eur. J. Appl. Math.*, **17** (2006), 257–292.

[7] R. Bürger, A. García, K. H. Karlsen and J. D. Towers, A family of numerical schemes for kinematic flows with discontinuous flux, *J. Eng. Math.*, **60** (2008), 387–425.

[8] R. Bürger, K. H. Karlsen, N. H. Risebro and J. D. Towers, Well-posedness in BV_t and convergence of a difference scheme for continuous sedimentation in ideal clarifier-thickener units, *Numer. Math.*, **97** (2004), 25–65.

[9] R. Bürger, K. H. Karlsen, H. Torres and J. D. Towers, Second-order schemes for conservation laws with discontinuous flux modelling clarifier-thickener units, *Numer. Math.*, **116** (2010), 579–617.

[10] R. Bürger, K. H. Karlsen and J. D. Towers, A model of continuous sedimentation of flocculated suspensions in clarifier-thickener units, *SIAM J. Appl. Math.*, **65** (2005), 882–940.

[11] R. Bürger, K. H. Karlsen and J. D. Towers, On some difference schemes and entropy conditions for a class of multi-species kinematic flow models with discontinuous flux, *Netw. Heterog. Media*, **5** (2010), 461–485.

[12] J. M. Coulson, J. F. Richardson, J. R. Backhurst and J. H. Harker, *Coulson and Richardson's Chemical Engineering. Volume 2: Particle Technology and Separation Processes*, Fourth Ed., Butterworth-Heinemann, Oxford, 2000.

[13] J. E. Dickinson and K. P. Galvin, Fluidized bed desliming in fine particle flotation, Part I, *Chem. Eng. Sci.*, **108** (2014), 283–298.

[14] S. Diehl, On scalar conservation laws with point source and discontinuous flux function, *SIAM J. Math. Anal.*, **26** (1995), 1425–1451.

[15] S. Diehl, A conservation law with point source and discontinuous flux function modelling continuous sedimentation, *SIAM J. Appl. Math.*, **56** (1996), 388–419.

[16] S. Diehl, Operating charts for continuous sedimentation I: Control of steady states, *J. Eng. Math.*, **41** (2001), 117–144.

[17] S. Diehl, Operating charts for continuous sedimentation II: Step responses, *J. Eng. Math.*, **53** (2005), 139–185.

[18] S. Diehl, A uniqueness condition for nonlinear convection-diffusion equations with discontinuous coefficients, *J. Hyperbolic Differential Equations*, **6** (2009), 127–159.

[19] S. Diehl, Numerical identification of constitutive functions in scalar nonlinear convection-diffusion equations with application to batch sedimentation, *Appl. Numer. Math.*, **95** (2015), 154–172.

[20] S. Diehl, S. Farås and G. Mauritsson, Fast reliable simulations of secondary settling tanks in wastewater treatment with semi-implicit time discretization, *Comput. Math. Appl.*, **70** (2015), 459–477.

[21] J. A. Finch and G. S. Dobby, *Column Flotation*, Pergamon Press, London, 1990.

[22] K. P. Galvin and J. E. Dickinson, bed desliming in fine particle flotation Part II: Flotation of a model feed, *Chem. Eng. Sci.*, **108** (2014), 299–309.

[23] S. K. Godunov, Finite difference methods for numerical computation of discontinuous solutions of equations of fluid dynamics, *Mat. Sb.*, **47** (1959), 271–306.

[24] H. Holden and N. H. Risebro, *Front Tracking for Hyperbolic Conservation Laws*, Second Edition, Springer Verlag, Berlin, 2015.

[25] P. M. Ireland and G. J. Jameson, Liquid transport in multi-layer froths, *J. Colloid Interf. Sci.*, **314** (2007), 207–213.

[26] S. N. Kružkov, First order quasilinear equations in several independent variables. *Math. USSR-Sb.*, **10** (1970), 217–243.

[27] D. E. Langberg and G. J. Jameson, The coexistence of the froth and liquid phases in a flotation column, *Chem. Eng. Sci.*, **47** (1992), 4345–4355.

[28] S. Mishra, Numerical methods for conservation laws with discontinuous coefficients, Chapter 18 in R. Abgrall and C.-W. Shu (eds.), *Handbook of Numerical Methods for Hyperbolic Problems: Applied and Modern Issues*, North Holland, **18** (2017), 479–506.

[29] G. Narsimhan, Analysis of creaming and formation of foam layer in aerated liquid, *J. Colloid Interface Sci.*, **345** (2010), 566–572.

[30] O. A. Oleinik, Uniqueness and stability of the generalized solution of the Cauchy problem for a quasi-linear equation *Uspekhi Mat. Nauk.*, **14** (1959), 165–170. *Amer. Math. Soc. Trans. Ser. 2*, **33** (1964), 285–290.

[31] R. Pal and J. H. Masliyah, Flow characterization of a flotation column, *Canad. J. Chem. Eng.*, **67** (1989), 916–923.

[32] R. Pal and J. H. Masliyah, Oil recovery from oil in water emulsions using a flotation column, *Canad. J. Chem. Eng.*, **68** (1990), 959–967.

[33] C.-H. Park, N. Subasinghe and O.-J. Han, Amenability testing of fine coal beneficiation using laboratory flotation column, *Materials Transactions*, **56** (2015), 766–773.

[34] J. F. Richardson and W. N. Zaki, Sedimentation and fluidisation: Part I, *Chemical Engineering Research and Design*, **75** (1997), 82–100.

[35] K. Rietema, Science and technology of dispersed two-phase systems—I and II, *Chem. Eng. Sci.*, **37** (1982), 1125–1150.

[36] A. Rushton, A. S. Ward and R. G. Holdich, *Solid-Liquid Filtration and Separation Technology*, Wiley Online Library, 2008.

[37] P. Stevenson, S. Ata and G. M. Evans, Convective-dispersive gangue transport in flotation froth, *Chem. Eng. Sci.*, **62** (2007), 5736–5744.

[38] P. Stevenson, P. S. Fennell and K. P. Galvin, On the drift-flux analysis of flotation and foam fractionation processes, *Canad. J. Chem. Eng.*, **86** (2008), 635–642.

[39] J. Vandenberghe, J. Chung, Z. Xu and J. Masliyah, Drift flux modelling for a two-phase system in a flotation column, *Canad. J. Chem. Eng.*, **83** (2005), 169–176.

[40] G. B. Wallis, *One-Dimensional two-Phase Flow*, McGraw-Hill, New York, 1969.

[41] G. B. Wallis, The terminal speed of single drops or bubbled in an infinite medium, *Int. J. Multiphase Flow*, **1** (1974), 491–511.

[42] B. A. Wills and T. J. Napier-Munn, *Wills' Mineral Processing Technology*, Seventh Edition, Butterworth-Heinemann, Oxford, 2006.

[43] J. B. Yianatos, J. A. Finch, G. S. Dobby and M. Xiu, Bubble size estimation in a bubble swarm, *J. Colloid Interf. Sci.*, **126** (1988), 37–44.

[44] Z. A. Zhou and N. O. Egiebor, A gas-liquid drift-flux model for flotation columns, *Minerals Eng.*, **6** (1993), 199–205.

E-mail address: rburger@ing-mat.udec.cl
E-mail address: stefan.diehl@math.lth.se
E-mail address: mmarti@ucsc.cl